

Kepler Eclipsing Binary Stars. VI. Identification of Eclipsing Binaries in the K2 Campaign 0 Data-set

Daryll M. LaCourse¹, Kian J. Jek¹, Thomas L. Jacobs¹, Troy Winarski¹, Tabettha S. Boyajian², Saul A. Rappaport³, Roberto Sanchis-Ojeda³, Kyle E. Conroy⁴, Lorne Nelson⁵, Tom Barclay⁶, Debra A. Fischer², Joseph R. Schmitt², Ji Wang², Keivan G. Stassun^{4,7}, Joshua Pepper⁸, Jeffrey L. Coughlin⁹, Avi Shporer^{10,11}, Andrej Prša¹²

ABSTRACT

The original *Kepler* mission observed and characterized over 2400 eclipsing binaries in addition to its prolific exoplanet detections. Despite the mechanical malfunction and subsequent non-recovery of two reaction wheels used to stabilize the instrument, the *Kepler* satellite continues collecting data in its repurposed *K2* mission surveying a series of fields along the ecliptic plane. Here we present an analysis of the first full baseline *K2* data release: the Campaign 0 data-set. In the 7761 light curves, we have identified a total of 207 eclipsing binaries. Of these, 97 are new discoveries that were not previously identified. Our pixel-level analysis of these objects has also resulted in identification of several false positives (observed targets contaminated by neighboring eclipsing binaries), as well as the serendipitous discovery of two short period exoplanet candidates. We provide catalog cross-matched source identifications, orbital periods, morphologies and ephemerides for these eclipsing systems. We also describe the incorporation of the *K2* sample into the Kepler Eclipsing Binary Catalog¹, present spectroscopic follow-up

¹Amateur Astronomer

²Department of Astronomy, Yale University, New Haven, CT 06511, USA

³Department of Physics, and Kavli Institute for Astrophysics and Space Research, Massachusetts Institute of Technology, Cambridge, MA 02139, USA

⁴Department of Physics and Astronomy, Vanderbilt University, VU Station B 1807, Nashville, TN 37235

⁵Department of Physics, Bishop's University, 2600 College St., Sherbrooke, QC J1M 1Z7

⁶NASA Ames Research Center, Moffett Field, CA 94035

⁷Department of Physics, Fisk University, Nashville, TN 37208, USA

⁸Department of Physics, Lehigh University, Bethlehem, PA 18015, USA

⁹SETI Institute/NASA Ames Research Center, Moffett Field, CA 94035, USA

¹⁰Jet Propulsion Laboratory, California Institute of Technology, Pasadena, CA 91109

¹¹NASA Sagan Fellow

¹²Department of Astrophysics and Planetary Sciences, Villanova University, 800 E Lancaster Ave, Villanova, PA 19085

¹keplerebs.villanova.edu/k2

observations for a limited selection of nine systems, and discuss prospects for upcoming *K2* campaigns.

Subject headings: catalogs: binaries - eclipsing, methods: data analysis, techniques: photometric

1. Introduction

Between 2009 and 2013, the *Kepler* space telescope recorded high-precision photometry almost continuously for more than 150,000 stars near the constellation Cygnus and Lyra (Koch et al. 2010; Borucki et al. 2011a,b; Batalha et al. 2013; Burke et al. 2014). This unprecedented data-set was used to detect more than 4000 exoplanet candidates (of which 1031 *Kepler* planets have been confirmed to-date) and revolutionized our understanding of the statistical occurrence of exoplanets and stellar astrophysics. The light curves of more than 2400 eclipsing binary stars were also measured (Prša et al. 2011; Slawson et al. 2011), resulting in the detection of over 70 triple systems (Rappaport et al. 2013; Conroy et al. 2014; Borkovits et al. 2015) and new astrophysical phenomena such as tidally excited Heartbeat binaries (Thompson et al. 2012), self-lensing binaries (Kruse et al. 2014), and Doppler boosting in ordinary stars (Kerkwijk et al. 2010).

Most of these discoveries were made by the *Kepler* science teams, using an automated pipeline (Jenkins et al. 2002, 2010) to analyze the photometric data. In addition, the Planet Hunters Citizen Science project² was established to engage the public in helping to analyze the wealth of light curves (Fischer et al. 2012). This turned out to be a complementary scientific asset: to date, the visual inspection of light curves from Planet Hunters has resulted in the recovery and characterization of many of the transiting systems detected by the *Kepler* team and more than 50 unique exoplanet candidates. This includes dozens of giant planet candidates residing in the putative habitable zones of their host stars, and a circumbinary exoplanet orbiting one of a pair of binaries in a widely separated quadruple system (Schwamb et al. 2013; Wang et al. 2013; Schmitt et al. 2014).

Kepler was about to begin an extended mission when the loss of the second of four reaction wheels ended the primary mission. At this juncture, a new plan of operation was devised to point the spacecraft along the ecliptic plane. This orbit minimizes the perturbations from solar illumination and pointing is maintained with the remaining two reaction wheels (Howell et al. 2014). This repurposed mission, known as *K2*, will survey ten new fields along the ecliptic plane over the next two to three years. Each of these ecliptic pointings constitutes one campaign, and the duration of observations for each field is limited to about 75 days because of solar radiation pressure constraints. All data are immediately non-proprietary, and will be released from the Mikulski Archive for Space Telescope (MAST) archive about three months after observations to engage the community in rapid

²www.planethunters.org

follow-up. The first *K2* observations began in 2014 March to assess the quality of the photometric precision. This Campaign 0 (C0) data was uploaded to MAST in 2014 September.

The *K2* C0 data set consists of observations from an ~ 80 day long engineering run, designed to assess whether a long term two-wheeled, ecliptic orientated mission was viable. Significant differences exist between the *Kepler* and the *K2* data sets in both quantity and quality. While the *Kepler* targets were carefully vetted before the launch of the mission and nominally selected based on their magnitude and luminosity class, the *K2* C0 targets were requested by the community and selected from 89 diverse Guest Observer proposals that aimed to carry out a broad range of science goals. This method of *K2* target selection has introduced different selection biases than for the stars observed in the *Kepler* field. The *K2* target information for each campaign is stored in the Ecliptic Plane Input Catalog³ (EPIC).

Unlike the *Kepler* mission, the quality of the *K2* C0 photometry is compromised by quasi-periodic, six hour thruster firings, a more rapidly changing thermal environment, and the emergent failure of detector Module 7. These effects have introduced significant and non-uniform systematics into the data. Targets that are farther from the bore sight sweep out larger arcs on the detectors than targets that are in the center of the field. Because of complications extracting and cleaning light curves, the *K2* mission is currently only providing MAST with a calibrated Target Pixel File (TPF) for each target.

Despite these new challenges, the precision photometry offered by the *K2* mission will continue to make significant contributions to the field of eclipsing binaries (EBs). This has already been evidenced by the ‘Two-Wheel Concept Engineering Test’ data set, a nine-day target limited observation performed in 2014 February that resulted in the detection of 31 EBs (Conroy et al. 2014). Upon release of the C0 TPFs, we developed a custom light curve extraction pipeline in order to reduce and review the data. We present results from our pilot study to identify light curves that exhibit periodic variations, in particular, eclipsing binaries in the C0 data set. These results join EBs detected from *Kepler* and the *K2*: Two-Wheel Concept Engineering Test within the Kepler Eclipsing Binary Catalog⁴.

2. Campaign 0 Light Curves

We initially extracted 7761 light curves in an automated fashion and independently de-correlated each of them against the spacecraft’s known pointing motions, using the same technique described in Vanderberg & Johnson (2014). In addition, the aperture extraction mask size was adjusted as a function of the EPIC catalog listed source magnitude, with minimum mask dimensions of 3×3 pixels designated for the faintest observed C0 targets (K_p of 19 or less) ranging up to 15×15 for the

³<http://archive.stsci.edu/k2/epic/search.php>

⁴<http://keplerebs.villanova.edu/>

brightest ($K_p \sim 9$). Unfortunately, a systemic spacecraft pointing error resulted in degradation for the first 40 days of observations for all targets (about half of the full C0 observation time baseline). While this early data range was not entirely compromised, we only used the second half of C0 observations in our bulk analysis. However, in our final analysis we were able to recover some of this early data to aid in characterizing several long period eclipsing binaries.

Visual inspection of the extracted C0 light curves produced an initial list of 258 EPIC targets that were flagged to be investigated for transient or periodic variations suggestive of an EB. A Fast Fourier Transform (FFT) routine subsequently recovered an additional 53 candidate signals of varying periods.

A 384,000 pixel ‘superstamp’ was used in C0 to capture flux from the open clusters NGC 2168 (M35) and NGC 2158. The superstamp is coverage oriented, and no explicit EPIC target identifications are associated with each of the 153 uniform dimension TPFs contained within the superstamp. We assessed each of the superstamp TPFs for crowding. In this selection, we excluded dim background sources comprised of fewer than four pixels and any brighter source truncated by the borders of the TPF mask. We tailored our photometric extraction routine to identify source centroids and process light curves, again adjusting aperture masks as a function of source magnitude. These superstamp extracted light curves were then visually reviewed and vetted at the pixel-level in the same manner as the regular C0 target sample. Although there is increased incidence of source confusion for superstamp TPFs covering the nominal center of each cluster, in many cases the exterior areas of the superstamp yielded high quality light curves at an average of 23 extractions per TPF. Examination of the output from this superstamp pipeline resulted in 49 additional periodic variables which were added to our initial investigation pool, bringing the total number of flagged targets to 360 .

Because of concern about the quality of the *K2* C0 data, we employed open source Guest Observer software PYKE (Still et al. 2012)⁵ to perform a second series of extractions for the flagged point sources, reducing the data into two new light curves using two different reduction techniques; Self Field Flattening (SFF) (Vanderberg & Johnson 2014) and Principal Component Analysis (PCA). These two reduction routines are included in the PYKE software package as KEPSFF and KEPPCA and have been updated for use with *K2*. The SFF method corrects for the *K2* aperture photometry artifacts by isolating short term variability and calculating a position-flux relation for each detrended iteration of the extracted light curve. PCA accomplishes a similar isolation of systematics by assessing the time series variability of each individual pixel in the chosen extraction mask and then segregating these trends into component groups that are correlated or anti-correlated to instrument movement (Harrison et al. 2012).

Aperture photometry pixel masks common to this second series of reductions and pixel level analysis were manually defined on a case by case basis in order to minimize flux losses from the

⁵<http://keplerscience.arc.nasa.gov/PyKE.shtml>

intended target and to exclude neighboring sources wherever possible. We also extracted and inspected light curves from bright neighboring sources that were potentially contaminating our target of interest.

The light curves extracted with KEPPCA and KEPSSF were compared to assess the degree each routine had muted or obfuscated the intrinsic astrophysical signal. Testing this across a variety of point sources showed that neither reduction technique offers a clear advantage over the other in all situations. As such, we chose to employ light curves derived from both KEPSSF and KEPPCA for each of the targets reviewed in the course of our dedicated pixel-level analysis.

3. Culling

Due to *Kepler*’s sensitivity, pixel size, and observing fields, the likeliness for source confusion common to any given target is high. The most common forms of contamination occur as a result of *Kepler*’s pixel response function (PRF), which is quantified by the spacecraft’s pointing precision, pixel resolution and point spread function (Bryson et al. 2010). When the PRF of two or more point sources directly overlap and blend, or when the PRF wings of sufficiently bright stars encroach into the photometric apertures of separated targets, the variable signal from one point source can be introduced into another point source as a diluted alias (Van Cleve et al. 2009; Caldwell et al. 2010). For this reason we take a conservative approach in the vetting of EBs for our final C0 sample. If the source of the eclipsing signal for a particular EB could not confidently be determined during a pixel level review, it was excluded from our final sample. Of the 360 light curves we flagged for eclipsing or ellipsoidal activity, 153 were ultimately rejected as spurious detections or blended binaries that could not be confidently associated with a specific point source. The itemized breakdown of these rejected EB candidates is detailed as follows:

1. Fifteen flagged EPIC targets were rejected as suspected cases of direct PRF contamination. Examination of the TPF in conjunction with review of optical all-sky databases (e.g., 2MASS, Skrutskie et al. 2006; DSS⁶; WISE, Wright et al. 2010) indicated that multiple point sources were blended or crowded within our initially employed photometric aperture. Subsequent efforts to re-extract and isolate the eclipse signal failed to tease apart the originating pixel location and as such these low signal-to-noise (SNR) candidates were culled from our sample.

2. Twenty-nine additional cases where a point source in the halo of an EPIC’s TPF was found to contaminate the intended EPIC target’s light curve. Aliases were identified where it was evident that the halo source displayed the same ephemerides but at a much greater amplitude. We have cross matched the 2MASS identifications of these non-EPIC EBs and appropriately noted the victimized EPICs as false positives in the KEPLER ECLIPSING BINARY CATALOG. In eight cases where the suspected source of contamination was truncated by the edge of the TPF definition or

⁶<https://archive.stsci.edu/dss/>

itself appeared to be a blend, the target was removed from our final sample.

3. Nine targets were culled after an investigation for periods and epochs that matched or were closely similar to another EB candidate in our sample. Ephemerides matching has previously proven an effective tool to root out false positives *Kepler* data (e.g., Batalha et al. 2013; Coughlin et al. 2014). With the small size of our vetting sample it was possible to perform this search manually with large allowances for period error. No maximum arc second search radius was imposed in order to safeguard against potential instrument related forms of contamination that allow variable signals to afflict victim sources positioned on entirely different area of the detector, such as CCD Crosstalk and Antipodal Reflection (Caldwell et al. 2010; Coughlin et al. 2014). Although no clear cases of such exotic contamination were clearly identified, we identified nine cases of EPICs that were contaminating other observed EPICs.

4. Fourteen pairs of EPICs were noted during ephemerides matching and other vetting processes as apparent duplicate observations: the TPFs for each EPIC center on the same apparent point source, but with minutely differing target catalog coordinates listed. After reviewing the data to ensure that a dim field companion star was not actually the source of either EPIC proposal, we retained the EPIC that appeared best centered on the intended target and removed the other seven EPICs from our sample.

5. Twenty-eight targets were rejected as cases of mistaken identity with variable stars displaying periodic or near-periodic pulsations or rotational modulation.

6. Sixty-five flagged EPICs were rejected without conclusive final dispositions and are suspected to be largely spurious detections from two general categories: faint background EBs unresolved in the TPF pixel data and available all-sky data or artifact escapements common to our reduction processes.

The 207 survivors of these culling reviews were selected for further characterization and calculation of ephemerides. A serendipitous by-product of these analyses were the identification of two exoplanet candidates.

4. Ephemerides, Periods, Phase Curves, Cross Matched Source Identifications, and Meta Data

The periodicity for each target displaying three or more eclipses was initially determined based on the phase dispersion minimization (PDM) method (Stellingwerf 1978). The PDM variant method described by Plavchan et al. 2008 was also used to find periods. The PDM methods essentially fold the light curve at different periods and assign a ‘dispersion score’ for each detected period. These scores are then sorted, the minima associated with the best scores are picked and iteratively phase folded at increasingly narrower period ranges to find the best local solution. Our routine based on the original Stellingwerf (1978) work proved effective at correctly identifying the

estimated period with no constraints on initial period range. However, we also utilized the PDM variant by (Plavchan et al. 2008) as it assigns scores differently: a boxcar average is subtracted from the flux for each test fold and the residuals are squared and summed in order to provide ranking.

We evaluated mid-eclipse times by employing the methods of ‘KWM’ (Kwee & van Woerden 1956), Barycenter (e.g., Oshagh et al. 2012) and Least Squares (e.g., Smith et al. 2012). The output parameters were then vetted by eye to ensure that BJD0 coincides with the deeper eclipse in cases where secondary eclipses are also present in the light curve.

We use these ephemerides to plot the EB phase curves, presented in Figures 1 through 12. The phase of each system is arranged for illustrative purposes such that the secondary eclipse, if present, is visible. The phase folded light curves were then used to determine a system morphology. Morphology values range between 0 (detached) and 1 (over-contact). Morphologies are determined by first fitting a chain of four quadratic functions to the shape of the phased light curve and then determining the morphology through application of a Local Linear Embedding Matijević et al. (2012) routine. With the exception of Heartbeat binaries and EBs lacking three observed eclipses, morphologies are computed for the entire C0 sample.

All targets observed eclipsing in the C0 data set were crossed matched against all-sky catalog listings in The International Variable Star Index (VSX) (Watson 2006) and the SIMBAD database (Wenger et al. 2000) within a 20 arc second search radius using RA and Dec coordinates from MAST. Results for 2MASS source identifications were found to be in good agreement with the K2-TESS stellar properties catalog (Stassun et al. 2014), which includes EPIC to 2MASS cross matches accurate to within one arc second. For M35 superstamp related targets, we also performed a cross check against recently published ground survey data from the Asiago Pathfinder for HARPS-N (APHN) program, which has performed a long term, high-precision (5 milli-mag) search of open clusters M35 and NGC 2158 for variable stars (Nardiello et al. 2014).

These cross matches allowed us to determine known stellar companions to our targets as well as alternate source identifications. We also checked and reviewed our results against the target proposal lists of the C0 Guest Observer (GO) proposals in order to determine which targets were known binary or multiple star systems. Our search of the GO proposals revealed that 110 of the 207 eclipsing targets we identified and retained in our final sample had been requested for *K2* C0 observation by several different GO programs as known or suspected binaries. An additional balance of 158 EPICs (approximately 60%) proposed by these binary star related GOs were not found to eclipse or possess ellipsoidal variations that could be attributed to a binary as per our culling criteria (Section 3). However a considerable portion of this balance may represent non-eclipsing objects (e.g., spectroscopic binaries, ELV binaries, cataclysmic variables, etc.) and thus the balance of non-detections in our *K2* C0 photometry is not unexpected.

Our analysis resulted in 97 new EBs detected in the C0 field. The orbital periods, ephemerides, morphologies, and cross matched identifications for all EBs in our sample are organized and presented in five tables. The 110 previously identified or suspected EBs in C0 are cataloged in Table 1.

The 97 new EB detections are presented in Table 2 (EPIC targets), Table 3 (M35 superstamp targets), and Table 4 (non-EPIC targets). The non-EPIC associated EBs were detected via their contamination of GO proposed target masks, creating a false positive EB signal. Due to the large size of C0 TPF stamps, we were able to extract and analyze light curves from these listed contaminants (see Section 3). A separate collection of false positive cases caused by direct pixel response function (PRF) contamination (Bryson et al. 2010) between pairs of observed EPIC targets are listed in Table 5.

The sky plotted distribution for all 207 EBs in our final sample is presented in Figure 13.

5. Spectroscopic Observations

We observed nine selected objects identified as interesting in our analysis (for details refer to Sections 7 and 8) on the nights of December 15, 19, and 20, 2014 using the Observatoire Astronomique du Mont-Mégantic’s (OMM) 1.6-m telescope and long-slit spectrometer. The spectrometer employed a 1200-line/mm grating which yielded a dispersion of $0.89 \text{ \AA}/\text{pixel}$ and a wavelength range of $\sim 1800 \text{ \AA}$ ($3750 - 5600 \text{ \AA}$). Depending on the brightness of each object, up to three exposures were co-added to improve the signal to noise; the total integration time for each object ranged between 20 to 90 minutes. All of the spectra were background subtracted, corrected for the quantum efficiency of the CCD detector and the reflectance of the grating, and corrected for Rayleigh scattering in the atmosphere before being co-added.

We classified the spectrum for each source by comparison to the Gray Digital Spectral Classification Atlas⁷ (Gray et al. 2009). We adopt a conservative uncertainty in the spectral classifications of 2 sub-classes. After a match in spectral type and luminosity class was found, we used the reference table in Boyajian et al. (2013) to estimate the fundamental stellar properties for each classification. The spectra are presented in Figure 14 (EBs) and Figure 16 (planet candidates). The spectrum for each target is discussed where appropriate in the sections to follow.

Nine stars for which we obtained spectroscopic T_{eff} estimate overlap in the K2-TESS portal. Eight of these nine stars have T_{eff} estimates in the K2-TESS database (Stassun et al. 2014). In all cases the photometric K2-TESS T_{eff} determination is significantly cooler than the spectroscopic based estimate of T_{eff} . Two of these stars are also present in the photometric catalog of all Tycho stars (Ammons et al. 2006), also having similar T_{eff} estimates as the K2-TESS estimates, though the Ammons et al. (2006) errors are typically on the order of several thousands of degrees (e.g., EPIC 202073097 has a $T_{\text{eff}} = 7418^{+4695}_{-447} \text{ K}$). We suspect that the reason for this disagreement is that reddening is not accounted for in the K2-TESS Catalog. Since the C0 field points to the galactic anti-center ($l \sim 190^\circ, b \sim 5^\circ$) and thus much through the galactic plane, reddening makes considerable differences in the target colors which are used in the color-temperature relations by the

⁷<https://ned.ipac.caltech.edu/level5/Gray/frames.html>

K2-TESS Catalog⁸. As such, any of the temperatures listed in this paper (not estimated from our spectra) should be used with caution. It is also worth noting that neither method makes correction for binarity, however this task is not trivial with the small amount of data at hand.

In any case, for this set of nine of spectroscopically observed stars, it appears that the K2-TESS dwarf/giant estimator method is reliable. Two stars that were observed spectroscopically were classified as likely giants (luminosity class III), and both of these were identified as giants also in the K2-TESS database on the basis of the reduced proper motion (see Stassun et al. 2014).

6. Ground-based Photometry

With a time baseline of about 80 days, the K2 light curves can be used to identify EBs with periods out to ~ 30 days. While K2 has greater detection capabilities than ground-based photometry, due to greater photometric precision and duty cycle, there is value in combining these results with those from ground-based photometric surveys and transit searches. Projects including SuperWASP (Pollacco et al. 2006; Hellier et al. 2011), HATNet (Bakos et al. 2004, 2013), XO (McCullough et al. 2005), and KELT (Pepper, et al. 2007; Pepper et al. 2012) have accumulated observations over many years, and provide greater time baselines than K2. The addition of longer time baselines to the K2 light curves makes it possible to search for eclipse timing variations or amplitude variations of the EBs.

To explore the potential of that approach, we have cross-matched the K2 EBs in Tables 1 and 2 with data from the KELT survey. KELT is a wide-field, small-aperture photometric survey, with a 23 degree x 23 degree field of view, and a nonstandard broad $V + I$ filter. Two of the currently reduced fields from KELT overlap with K2 C0 north of $\text{Dec} = +19^\circ$. The KELT light curves were reduced and extracted according to the procedures described in Siverd et al. (2012), and include about 7700 to 8600 observations from Oct 2006 to March 2013. Additional observations after that time have been gathered but not yet reduced. Typical photometric precisions are 0.5% rms around $V = 9^{th}$ magnitude, and 2% rms around $V = 12^{th}$ magnitude. North of $+19$ degrees, KELT has light curves for all K2 C0 targets brighter than 12^{th} magnitude, and has light curves for at least 50% of the K2 C0 targets in the range $12 < V < 13$.

The long time baseline and good photometric precision of the KELT light curves allow us to measure the properties of many of the eclipsing binaries found in K2. A full analysis is ongoing, but we show an example of combining the KELT and K2 data in Figure 15. Table 6 displays the overlap of targets with K2 C0 and the currently available KELT data in hand. Potential applications include searching for eclipse depth, duration, and timing variations indicative of outer companions, or placing upper limits on such variations.

⁸Dereddened T_{neff} 's are now available in the K2-TESS portal. These results generally perform better, though several hundreds of K differences from the spectroscopic values still remain in some cases.

7. Noteworthy EBs

Noteworthy EBs within our final sample include ten detached eclipsing binaries with periods longer than 20 days (EPICs: 202064253, 202071945, 202072282, 202084588, 202086225, 202090938, 202091197, 202091404, 202092842, 202071645) and six candidates possessing single eclipses of significant depth but for which no period is yet determined (EPICs: 202060921, 202071902, 202072917, 202085278, 202135247, 202137580). We have also discovered six ‘Heartbeat binaries’ (e.g., Welsh et al. 2011; EPICs: 202060503, 202064080, 202065802, 202065819, 202071828, 202072282); see Figure 17. The most eccentric binaries, identified from the phase difference of the observed primary and secondary minimas, are presented in Table 7.

The following is a brief discussion on ten notable EBs in our sample. Their full light curves are presented in Figures 18 and 19. Figure 14 shows the spectrum of the object, if available (Section 5).

- **EPIC 202073097** A GO proposed EB with a period of 0.97 days and associated with a point source of *Kepler* magnitude $K_p = 9.6$. Alternate designations for EPIC 202073097 include HD 251042 and 2MASS 06042191+2032032. The C0 light curve shows a second set of eclipses of similar depth and duration with a period of 5.33 days. The five day period is not observed in extractions from the halo pixel sources within the TPF for EPIC 202073097. It is unclear if this anomaly represents two independent binaries or a gravitationally bound pair of binaries in a quadruple system. Spectral analysis indicates a late A1 or A0 component is present, possibly evolved as Fe II and Si II are observed. This is consistent with the The Henry Draper Catalogue classification of A2 (Cannon & Pickering 1993).
- **EPIC 202073145** A GO proposed EB with a period of 1.52 days, 30% depth, and $K_p = 11.3$. The light curve also displays an additional anomalous signal with a depth of 15% and a period of 4.44 days. Alternate designations for EPIC 202073145 include TYC 1323-169-1 and 2MASS 06185463+2036038. It is unclear solely from a pixel-level review if the longer period represents a close background contaminator or a second binary in a quadruple system. The K2-TESS Catalog lists $T_{\text{eff}} = 6208$ K for this source; our spectrum indicates a considerably hotter B3V type star, which is assumed to be un-evolved due to the absence of O II.
- **EPIC 202088178** A new EB from this paper with a period of 2.37 days, 15% depth, and $K_p = 13.3$. EPIC 202088178 is also known as 2MASS 06230702+1828149. An additional series of eclipses are observed with a shorter period of 0.49 days, and a depth of only 0.5%. A pixel-level review was inconclusive but cannot rule out with confidence that the light curve contains two unresolved binary systems. The K2-TESS Catalog lists $T_{\text{eff}} = 5270$ K for this source. Our OMM spectrum indicates the star has a true temperature much higher with a spectral type of F5 II.
- **EPIC 202092613** A new EB with two periodic signals: a 3.18 day period with a primary eclipse depth of 5%, and a 0.25-day periodic modulation with an amplitude of 0.5%. . The

additional short period signal is not resonant with the 3.18 day period, and we suspect the cause of this 0.5% amplitude modulation is attributed to either pulsations or star spots common to one of the binary components. We classify the OMM spectrum of this object as a A0V based on Balmer line strengths, weak Mg II ratio and lack of Si II in the OMM spectrum. If the observed short period variability is driven by star spots, it could indicate a rapid rotation period of ~ 6 hours. However, given the stellar effective temperature and ratio of eclipse depths it is more likely that the short period signal represents pulsations.

- **EPIC 202088387** A new EB with a period of 3.55 days, depth of 15%, and $K_p = 12.9$. Alternate designations for EPIC202088387 include 2MASS 06064169+2234547 and SDSS J060641.69+223454.8. The light curve also exhibits asymmetrical brightening events of ~ 2 days duration with an amplitude $\sim 5\%$, which we assume to be associated with nearly co-rotating starspots or pulsations in one of the stellar components. The K2-TESS Catalog $T_{\text{eff}} = 5652$ K; we do not have a spectrum of this object to confirm this temperature.
- **EPIC 202135247** A new EB ($K_p = 14.4$; also known as 2MASS 06195142+1747474) with unknown period – a single, flat-bottomed, 9% eclipse depth with a duration of 35 hours is observed. The K2-TESS Catalog lists $T_{\text{eff}} = 3919$ K. Our OMM spectrum suggests an earlier-type primary component of G1.5. While the G-band strengths in our spectrum could be representative of either a luminosity class of V or III, the eclipse profile suggests an evolved star and annular eclipse of a smaller stellar companion.
- **EPIC 202137580** A new EB ($K_p = 13.1$; also known as 2MASS 06031044+2330174) with unknown period. The light curve has a single 7% flat bottomed eclipse with a 37 hour duration. While it has a similar eclipse profile to EPIC 202135247 (above) which may suggest an evolved component, the observed impact durations are considerably different as evidenced by shorter ingress and egress coupled to a longer disc passage of 28 hours. With our OMM spectrum, we classify the primary component as G0, much hotter than $T_{\text{eff}} = 3755$ K from the K2-TESS Catalog. The evolutionary state of this target is unclear as the strength of the G-band in our spectrum rules out a supergiant, but does support either luminosity class V or III. An unexplained long term trend in the light curve is visible and may be associated with orbital modulation and a period of under ~ 100 days.
- **EPIC 202062176** An eccentric (Table 7), new EB also known as 2MASS 06095262+2030273 having a period of 4.35 days, eclipse depth of $\sim 3.5\%$, and $K_p = 11$. Independently proposed by two GO programs for massive stars and a third for exoplanet detection, this EPIC may be a member of NGC 2174/2175.
- **EPIC 202072430** Also known as TYC 1330-2152-1 and 2MASS 06402451+1508324, EPIC 202072430 is one of the ten longest period eclipsing binaries identified in our sample with $P = 20.03$ days. This eccentric (Table 7) EB has a $K_p = 10.9$ and 45% primary eclipse depths. Two orbital cycles are captured in the C0 data; the light curve exhibits additional quasi-periodic variability in the out of eclipse regions on the order of ~ 8 hours.

- **EPIC 202068807** EPIC 202068807 ($K_p = 12.01$), also known as TYC 1878-947-1 and 2MASS 06204185+2317264 is a new, eccentric (Table 7), EB with a 4.24 day period. The light curve has primary and secondary eclipse depths of ~ 12 and 4%, respectively. This eccentric binary displays out-of-eclipse asymmetrical ellipsoidal variation at the 0.5% level.

8. Exoplanet Candidates

We report the detections of transiting planet candidates in the *K2* C0 data set: EPIC 202072704, and 2MASS 06101557+2436535 (no EPIC assignment as of this writing). The light curves for these objects were initially detected via the processing methods described in Section 2. After a detailed search of the TPF to rule out obvious contamination effects from other sources, the light curves were normalized and detrended specifically for analysis using the Transit Analysis Package (Gazak et al. 2012) in order to make a preliminary validation of their sub-stellar nature. HAT-P-54b, recently discovered by (Bakos et al. 2014), was also identified in our analysis, but we do not elaborate upon it here.

In an effort to better characterize the candidate host stars in our orbital fits, we obtained a spectrum of each of the new planet candidate host stars (excluding HAT-P-54b) with the OMM spectrograph (see Section 5 for details). The spectra reveal that the hosts are early-type stars. Our best-fit transit model retains a sub-stellar nature for each of the transiting companions, and we consider them new *K2* objects of interest worthy of further follow up. The candidates common to these systems are of particular interest as there are currently few confirmed examples in the literature of exoplanets transiting early-type stars (e.g., WASP-33 Collier-Cameron et al. 2010, and Kepler-13 Shporer et al. 2011, 2014).

The orbital solutions for each C0 candidate are shown in Table 8 and the phase-folded transit fits are shown in Figure 16 with the spectrum of each point source.

- **EPIC 202072704** This host star candidate has a $K_p = 11.4$, with alternate designations including HD 263309 and 2MASS 06455102+1712250. We identify twelve transit events of 3.16 hours duration, depths of 6588 ppm, and a period of 2.65 days. There are no apparent contaminating sources within the TPF halo. The OMM spectrum suggests the host star is an A3V, consistent with the Henry Draper Catalogue classification of A5 (Cannon & Pickering 1993). Using the tables from Pecaute & Mamajek (2013), we assume the host has a nominal radius of $1.7 R_\odot$. A best fit transit model based on these parameters indicates the transiting object has a radius of $1.26 R_{\text{Jup}}$ ($14.1 R_\oplus$) and orbital radius of 0.04 AU.
- **2MASS 06101557+2436535** Located within the first listed TPF (200000811) for the M35 star cluster super stamp, a transit signal is recovered from a $V = 12.6$ point source associated with pixel coordinates corresponding to column number 52 and row number 36. This source has been cross matched to 2MASS 06101557+2436535, as well as KIC 27058 from the original

Kepler Input Catalog, although it lies out of the *Kepler* field of view (Brown et al. 2011). The light curve for this source displays five transits with a period of 7.5559 days, and depths of 6928 ppm. We are able to recover two additional transits of acceptable quality in the early coarse point data. Using the OMM spectrum, we classify this source as an A2IV/V star. Assuming a stellar radius of $1.8 R_{\odot}$ (Pecaut & Mamajek 2013), our best fit transit model results in a planet radius of $1.37 R_{\text{Jup}}$ ($14.50 R_{\oplus}$) object orbiting at a separation of 0.08 AU. Further stellar characterization is needed to determine the evolutionary state of the host star, as its radius is quite uncertain.

In addition to these planet candidates, EPIC 202066192 and EPIC 202090723 were initially noted as potential candidates. However, EPIC 202066192, was ultimately rejected as a false positive due to a V-shaped eclipse profile, high impact parameter, and early-type A0III-IV OMM spectral classification. EPIC 202090723’s spectral type is determined from our OMM spectrum to be F5V – perfect agreement with the F5V classification from McCuskey (1967). Although the best fit transit model resulted in a planet radius of $\sim 0.5 R_{\text{Jup}}$, a single high-resolution TRES spectrum showed signs of a secondary in the line profile (D. Latham, private communication). Note that our spectral classification infers a source about a thousand degrees hotter than the K2-TESS Catalog estimate of $T_{\text{eff}} = 5442$ K, similar to other discrepancies identified in this paper.

9. Eclipse Timing Variations (ETVs)

Eclipse Timing Variations (ETVs) can be induced by the gravitational presence of a third object in a system (Conroy et al. 2014). Particularly so for short period binaries, the hierarchical triple system occurrence rate is estimated to be 40% or greater (Tokovinin et al. 2006). The Kepler Eclipsing Binary Catalog provides comprehensive eclipse timings from which over 100 confirmed and candidate triple systems have been identified (see also Rappaport et al. 2013; Borkovits et al. 2015).

Using the periods and ephemerides derived in Section 4, we analyzed the C0 light curves for a deviation from a strictly linear ephemeris within the threshold of *K2*’s 30 minute observation cadence. This analysis resulted in several C0 EBs that display intriguing low amplitude trends and sinusoidal variations. However, these observed effects could be driven by interactions that do not require a third object (e.g. dynamical mass transfer, quadrupole coupling, apsidal motion; Conroy et al. 2014). We are further burdened by the limited baseline for C0, in that most third body ETVs exhibit an O-C residual period greater than 45 days (Rappaport et al. 2013). This makes it unlikely for a full ETV cycle to have been serendipitously captured for a given target. We conclude that our analyses returned no high confidence ETV periods that clearly suggest the presence of a third body companion.

10. Summary and Discussion

Despite the new challenges inherent in working with currently available *K2* data, the overall quality of these light curves, when properly decorrelated, is still well suited for the detection of eclipsing binaries. A total of 207 eclipsing binaries are recovered by visual inspection of the *K2* C0 data set. For the 97 newly identified EBs, we provide periods, ephemerides, and cross-matched catalog identifications. Due to the shorter baseline of C0 compared to the *Kepler* data set, the balance of detected eclipsing systems is unsurprisingly dominated by short period binaries, with a steep rise in EBs with periods of less than five days. Of 207 systems identified in the *K2* C0 data, 58 have periods in excess of five days. The majority of these (42 systems) are previously undetected with ground photometry (Table 2). The Kepler Eclipsing Binaries Catalog has been expanded to include all EPIC EBs⁹ in the C0 field with three or more observed eclipses. The EPICs contaminated by neighboring EBs are cataloged as false positives in the Kepler Eclipsing Binary Catalog, having identifiers associated with the EPIC target that led to their detection.

The period distribution for the *K2* C0 EBs with orbital periods less than 25 days is displayed in Figure 20. Due to unknown selection biases it is not possible to evaluate incompleteness or draw firm conclusions regarding the fractional occurrence of EBs found in the C0 data set. Overall occurrence rate for all EBs in our *K2* C0 sample is noted at 2.5%, which is slightly higher than the 1.6% determined for *Kepler*. Despite this, we detect an underrepresented range of EBs with periods of less than one day; the cause of this shortage is currently unknown but likely to be influenced by GO target selection bias and the self-imposed limitations of our own selection processes. We further recognize that the decorrelation methods utilized in our survey have played a major role in our recovery ratios and overall completeness. While KEPSFF and KEPPCA provide an excellent foundation from which to reduce *K2* data, intrinsic astrophysical signals can be obfuscated or removed by such solutions and care must be taken in their application. Alternative approaches to mitigating the effect of spacecraft pointing jitter are being explored, such as those described by Aigrain et al. (2015) and Foreman-Mackey et al. (2015).

There are compelling incentives that encourage the community to analyze each incoming *K2* Campaign data set in a diligent and timely manner in order to characterize new eclipsing binary and exoplanet candidates, particularly in cases where the host star is bright or close. Many such systems are within reach from the ecliptic and *K2* stands uniquely poised to provide high precision photometry for a limited selection of targets with overlapping coverage common to the upcoming TESS (Ricker et al. 2014) mission, which will begin an all sky survey little more than one year after the currently scheduled conclusion of *K2* operations. For such systems meeting TESS selection criteria, the *K2* campaign baseline of 80 days will provide expanded pre-coverage that should serve to make prospective detections of long period objects (e.g., objects that transit only once or twice in a *K2* baseline) whose signals might conceivably manifest themselves as transient dimming events

⁹keplerebs.villanova.edu/k2

during ecliptic-orientated TESS observations. While *K2* observations alone cannot fully characterize such long period events, their initial identification will allow potential spectroscopic or photometric follow-up from ground based or in-orbit facilities.

In addition, any M or K dwarfs local to Earth (e.g. within 20 parsecs) that can be shown to be binaries or blended binaries via *K2* photometry (or subsequent ground based follow-up) constitute a limited yet important early sample from a population of high priority targets for the upcoming JWST mission. Owing to their reduced stellar radii, transits and eclipses occurring in such systems can yield significantly higher final average SNR values and in some cases allow limited transmission spectroscopy. However, by consequence, the deeper transits noted for such stellar types must be carefully vetted against the host of false positive possibilities. The JWST Continuous Viewing Zone will have some degree of overlap with *K2* ecliptic fields, but the instrument will also possess a finite supply of thruster fuel. Thus, it is critical that no exoplanet follow-up observations be squandered on a previously unidentified EB or BGEB.

Note Added in Manuscript: Since our paper was essentially completed, we have learned of a related study of the *K2* Field 0 by (Armstrong et al. 2015). The K2 VARIABLE CATALOG II lists 2619 Field 0 variable objects including 137 EBs, but used a qualitatively different detrending algorithm than we have employed and does not include full ephemerides or cross matched identifications.

Funding for the *Kepler* and *K2* Discovery missions is provided by NASAs Science Mission Directorate. TSB, DAF, JW, and JRS acknowledge support provided through NASA grant ADAP12-0172 and ADAP14-0245. LN thanks the Natural Sciences and Engineering Research Council (NSERC) of Canada for financial support, and the staff at the Observatoire Astronomique du Mont-Mégantic for their technical assistance. Some of the data presented in this paper were obtained from the Mikulski Archive for Space Telescopes (MAST). STScI is operated by the Association of Universities for Research in Astronomy, Inc., under NASA contract NAS5-26555. Support for MAST for non-HST data is provided by the NASA Office of Space Science via grant NNX13AC07G and by other grants and contracts. This research has made use of the NASA Exoplanet Archive, which is operated by the California Institute of Technology, under contract with the National Aeronautics and Space Administration under the Exoplanet Exploration Program. This research has made use of the VizieR catalogue access tool, CDS, Strasbourg, France. The original description of the VizieR service was published in Ochsenbein et al. (2000). This research has made use of the SIMBAD database, operated at CDS, Strasbourg, France (Wenger et al. 2000). This research has made use of the International Variable Star Index (VSX) database, operated at AAVSO, Cambridge, Massachusetts, USA. This publication makes use of data products from the Two Micron All Sky Survey, which is a joint project of the University of Massachusetts and the Infrared Processing and Analysis Center/California Institute of Technology, funded by the National Aeronautics and Space Administration and the National Science Foundation. This publication makes use of data products from the Wide-field Infrared Survey Explorer, which is a joint project of the University of California, Los Angeles, and the Jet Propulsion Laboratory/California Institute of Technology,

funded by the National Aeronautics and Space Administration. The Digitized Sky Surveys were produced at the Space Telescope Science Institute under U.S. Government grant NAG W-2166. The images of these surveys are based on photographic data obtained using the Oschin Schmidt Telescope on Palomar Mountain and the UK Schmidt Telescope. The plates were processed into the present compressed digital form with the permission of these institutions.

The authors gratefully acknowledge Ball Aerospace, the Kepler/K2 team and the Guest Observer community for making the *K2* mission possible.

Facilities: Kepler/K2, Observatoire Astronomique du Mont-Mégantic’s (OMM)

REFERENCES

- Aigrain, S., Hodgkin, S. T., Irwin, M. J., et al. 2015, MNRAS, 447, 2880
- Ammons, S. M., Robinson, S. E., Strader, J., et al. 2006, ApJ, 638, 1004
- Armstrong, D. J., Kirk, J., Lam, K. W. F., et al. 2015, arXiv:1502.04004
- Bakos, G., Noyes, R. W., Kovács, G., et al. 2004, PASP, 116, 266
- Bakos, G. Á., Csubry, Z., Penev, K., et al. 2013, PASP, 125, 154
- Bakos, G. Á., Hartman, J. D., Bhatti, W., et al. 2014, arXiv:1404.4417
- Batalha, N. M., Rowe, J. F., Bryson, S. T., et al. 2013, ApJS, 204, 24
- Borucki, W. J., Koch, D. G., Basri, G., et al. 2011, ApJ, 728, 117
- Borucki, W. J., Koch, D. G., Basri, G., et al. 2011, ApJ, 736, 19
- Borkovits, T., Rappaport, S., Hajdu, T., & Sztakovics, J. 2015, MNRAS, 448, 946
- Boyajian, T. S., von Braun, K., van Belle, G., et al. 2013, ApJ, 771, 40
- Brown, T. M., Latham, D. W., Everett, M. E., & Esquerdo, G. A. 2011, AJ, 142, 112
- Bryson, S. T., Tenenbaum, P., Jenkins, J. M., et al. 2010 ApJ, 713, L97
- Burke, C. J., Bryson, S. T., Mullally, F., et al. 2014, ApJS, 210, 19
- Caldwell, D. A., van Cleve, J. E., Jenkins, J. M., et al. 2010, Proc. SPIE, 7731, 773117
- Cannon, A. J., & Pickering, E. C. 1993, VizieR Online Data Catalog, 3135, 0
- Collier Cameron, A., Guenther, E., Smalley, B., et al. 2010, MNRAS, 376, 1424
- Christian, D. J., Pollacco, D. L., Skillen, I., et al. 2006, MNRAS, 372, 1117

- Conroy, K. E., Prša, A., Stassun, K. G., et al. 2014, *AJ*, 147, 45
- Conroy, K. E., Prša, A., Stassun, K. G., et al. 2014, *PASP*, 126, 914
- Coughlin, J. L., Thompson, S. A., Bryson, S. T., et al. 2014, *ApJ*, 147, 119
- Fischer, D. A., Schwamb, M. E., Schawinski, K., et al. 2012, *MNRAS*, 419, 2900
- Foreman-Mackey, D., Montet, B. T., Hogg, D. W., et al. 2015, arXiv:1502.04715
- Gazak, J. Z., Johnson, J. A., Tonry, J., et al. 2012, *Advances in Astronomy*, 2012, 697967
- Gray, R. O., & Corbally, C., J. 2009, *Stellar Spectral Classification by Richard O. Gray and Christopher J. Corbally*. Princeton University Press, 2009. ISBN: A 978-0-691-12511-4
- Harrison, T. E., Coughlin, J. L., Ule, N. M., & López-Morales, M. 2012, *AJ*, 143, 4
- Hellier, C., Anderson, D. R., Collier Cameron, A., et al. 2011, *European Physical Journal Web of Conferences*, 11, 01004
- Howell, S. B., Sobeck, C., Haas, M., et al. 2014, *PASP*, 126, 398
- Jenkins, J. M., Caldwell, D. A., Borucki, W. J. 2002, *ApJ*, 564, 495
- Jenkins, J. M., Caldwell, D. A., Chandrasekaran, H., et al. 2010, *ApJ*, 713, 87
- van Kerkwijk, M. H., Rappaport, S. A., Breton, R. P., et al. 2010 *ApJ* 715, 51
- Kinemuchi, K., Barclay, T., Fanelli, M., et al. 2012, *PASP*, 124, 963
- Koch, D. G., Borucki, W. J., Basri, G., et al. 2010, *ApJ* 713, 79
- Kruse, E., & Agol, E. 2014, *Science*, 344, 275
- Kumar, P., Ao, C. O., & Quataert, E. J. 1995, *ApJ*, 449, 294
- Kwee, K. K., & van Woerden, H. 1956, *Bull. Astron. Inst. Netherlands*, 12, 327
- Matijević, G., Prša, A., Orosz, J. A., et al. 2012, *AJ*, 143, 123
- McCullough, P. R., Stys, J. E., Valenti, J. A., et al. 2005, *PASP*, 117, 783
- McCuskey, S. W. 1967, *AJ*, 72, 1199
- Mighell, K. J. & Plavchan, P. 2013, *AJ*, 145, 148
- Mikulášek, Z., Chrastina, M., Liška, J., et al. 2014, *Contributions of the Astronomical Observatory Skalnaté Pleso*, 43, 382
- Nardiello, D., Bedin, L. R., Nascimbeni, V., et al. 2014, *MNRAS*, 447, 3536

- Ochsenbein, F., Bauer, P., & Marcout, J. 2000, *A&AS*, 143, 23
- Oshagh, M., Boué, G., Haghighipour, N., Montalto, M., et al. 2012, *A&A*, 540, A62
- Pecaut, M. J., & Mamajek, E. E. 2013, *ApJS*, 208, 9
- Pepper, J. Pogge, R. W., DePoy, D. L., et al. 2007, *PASP*, 119, 923
- Pepper, J., Kuhn, R. B., Siverd, R., James, D., & Stassun, K. 2012, *PASP*, 124, 230
- Plavchan, P., Jura, M., Kirkpatrick, J. D., et al. 2008, *ApJS*, 175, 191
- Pollacco, D. L., Skillen, I., Collier Cameron, A., et al. 2006, *PASP*, 118, 1407
- Prša, A., Batalha, N., Slawson, R. W., et al. 2011, *AJ*, 141, 83
- Prša, A., Matijević, G., & Conroy, K. 2015, in prep.
- Rappaport, S., Deck, K., Levine, A., et al. 2013, *ApJ*, 768, 33
- Ricker, G. R., Winn, J. N., Vanderspek, R., et al. 2014, *Proceedings of the SPIE*, 9143, 914320
- Rowe, J. F., Bryson, S. T., Marcy, G. W., et al. 2014, *ApJ*, 784, 45
- Schwamb, M. E., Orosz, J. A., Carter, J. A., et al. 2013, *ApJ*, 768, 127
- Schmitt, J. R., Wang, J., Fischer, D. A., et al. 2014, *AJ*, 148, 28
- Shporer, A., Jenkins, J. M., Rowe, J. F., et al. 2011, *AJ*, 142, 195
- Shporer, A., O’Rourke, J. G., Knutson, H. A., et al. 2014, *ApJ*, 788, 92
- Siverd, R. J., Beatty, T. G., Pepper, J., et al. 2012, *ApJ*, 761, 123
- Skrutskie, M. F., Cutri, R. M., Stiening, R., et al. 2006, *AJ*, 131, 1163
- Slawson, R. W., Prša, A., Welsh, W. F., et al. 2011, *AJ*, 142, 160
- Smith, J. C., Stumpe, M. C., Van Cleve, J. E., et al. 2012, *PASP*, 124, 1000
- Stassun, K. G., Pepper, J. A., Paegert, M., De Lee, N., & Sanchis-Ojeda, R. 2014, *arXiv:1410.6379*
- Stellingwerf, R. F. 1978, *ApJ*, 224, 953
- Still, M., & Barclay, T. 2012, *Astrophysics Source Code Library*, 1208.004
- Thompson, S. E., Everett, M., Mullally, F., et al. 2012, *ApJ*, 753, 86
- Tokovinin, A., Thomas, S., Sterzik, M., & Udry, S. 2006, *A&A*, 450, 681
- Wang, J., Fischer, D. A., Barclay, T., et al. 2013, *ApJ*, 776, 10

- Watson, C. L. 2006, Society for Astronomical Sciences Annual Symposium, 25, 47
- Welsh, W. F., Orosz, J. A., Aerts, C., et al. 2011, ApJS, 197, 4
- Wenger, M., Ochsenbein, F., Egret, D., et al. 2000, A&AS, 143, 9
- Wright, E. L., Eisenhardt, P. R. M., Mainzer, A. K., et al. 2010, AJ, 140, 1868
- Vanderberg, A. & Johnson, J. A. 2014, PASP, 126, 948
- Van Cleve, J. E. & Caldwell, D. A. 2009, ApJ, 142, 160

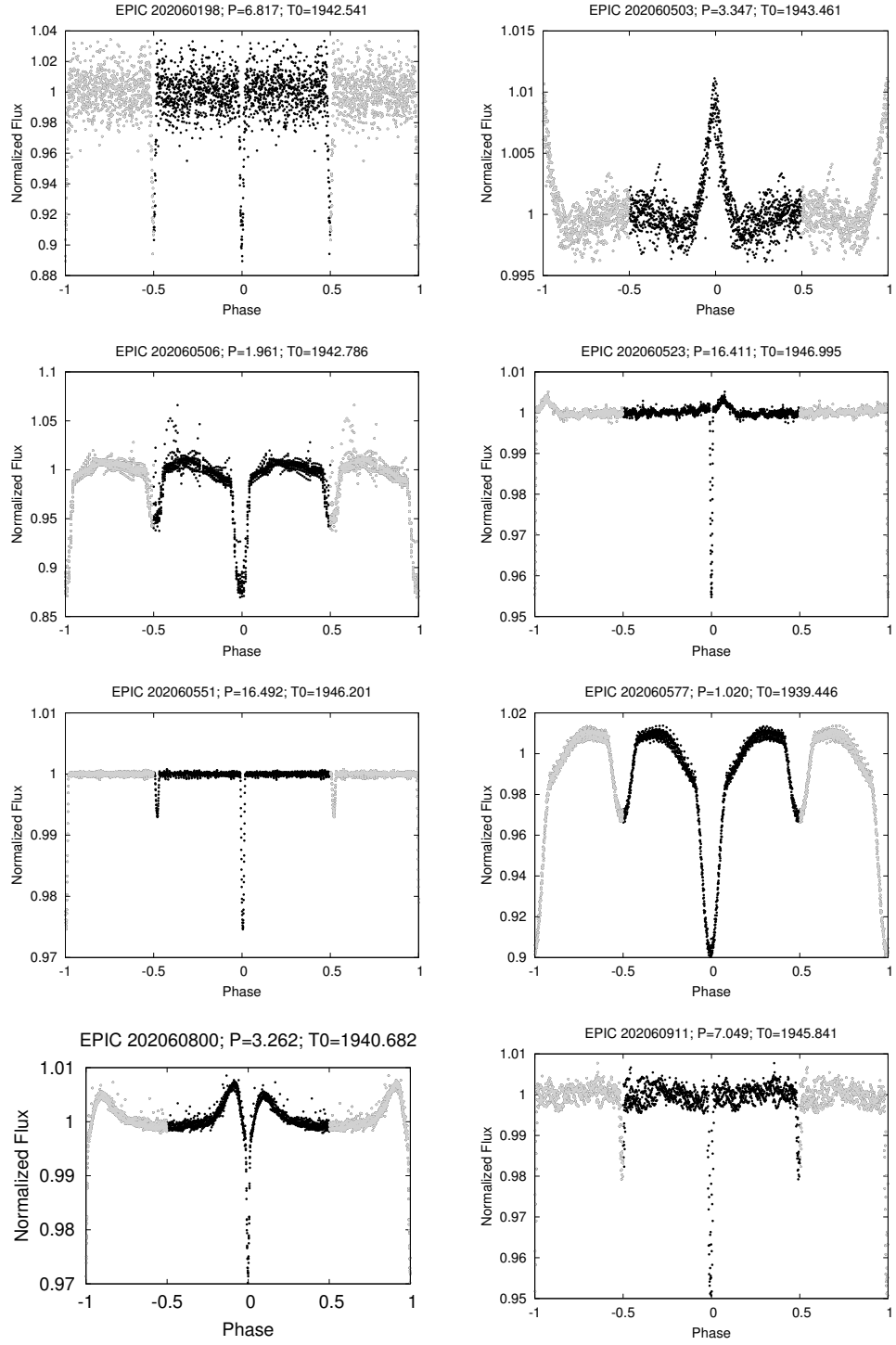


Fig. 1.— Plots of phased light curves for new eclipsing systems. Ephemerides are presented in Tables 2, 3, and 4. See Section 4 for details.

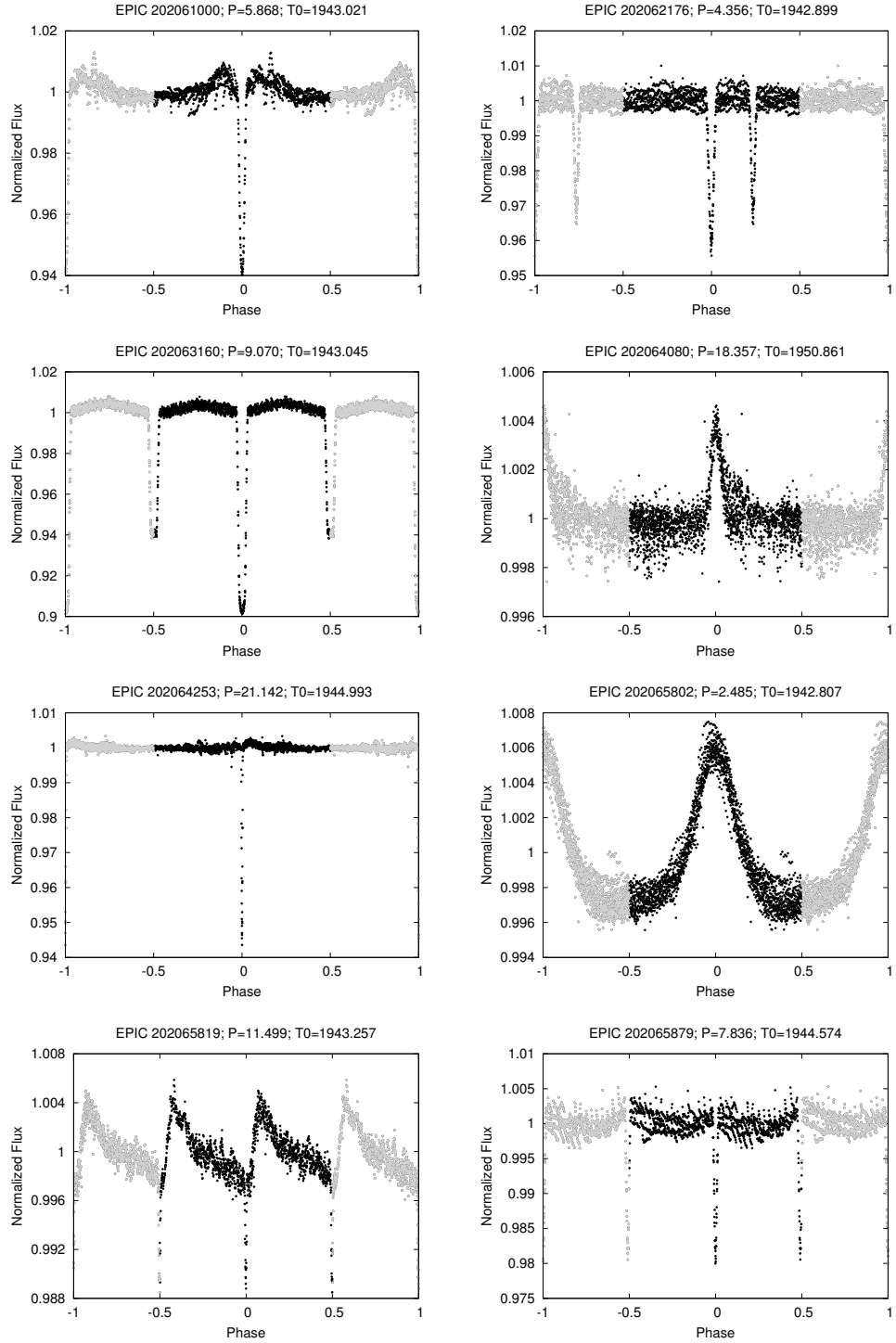


Fig. 2.— Plots of phased light curves for new eclipsing systems. Ephemerides are presented in Tables 2, 3, and 4. See Section 4 for details.

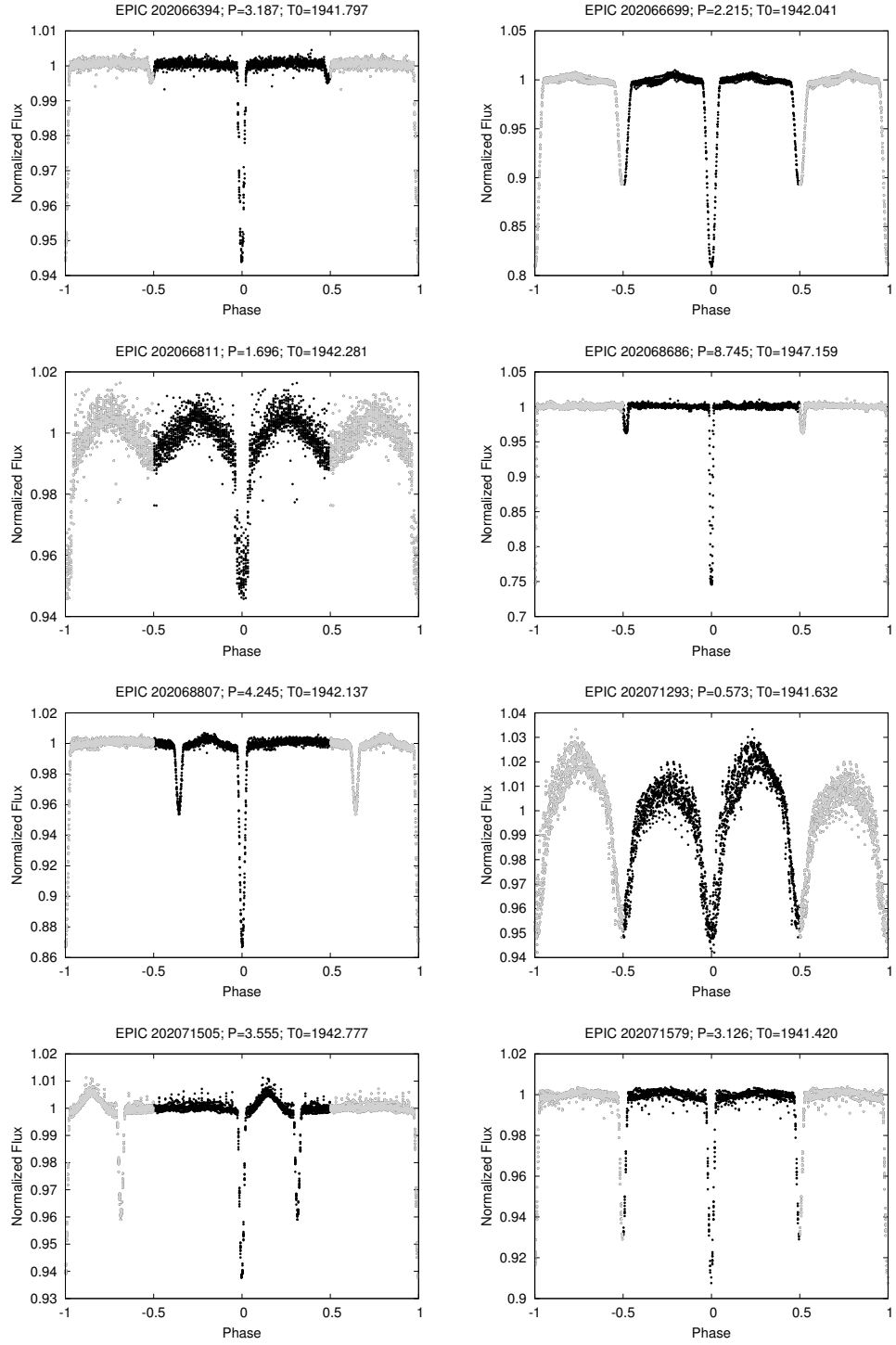


Fig. 3.— Plots of phased light curves for new eclipsing systems. Ephemerides are presented in Tables 2, 3, and 4. See Section 4 for details.

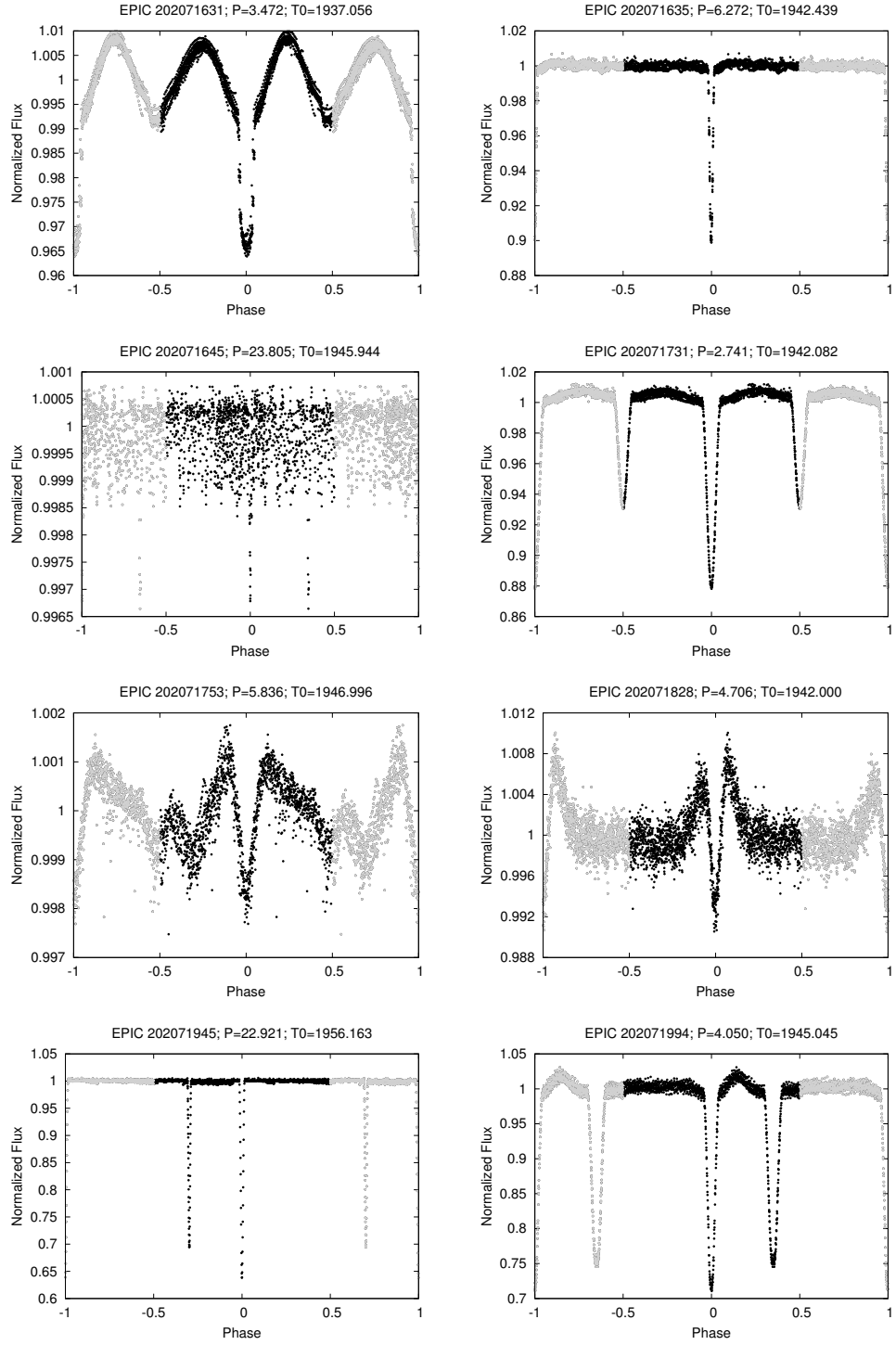


Fig. 4.— Plots of phased light curves for new eclipsing systems. Ephemerides are presented in Tables 2, 3, and 4. See Section 4 for details.

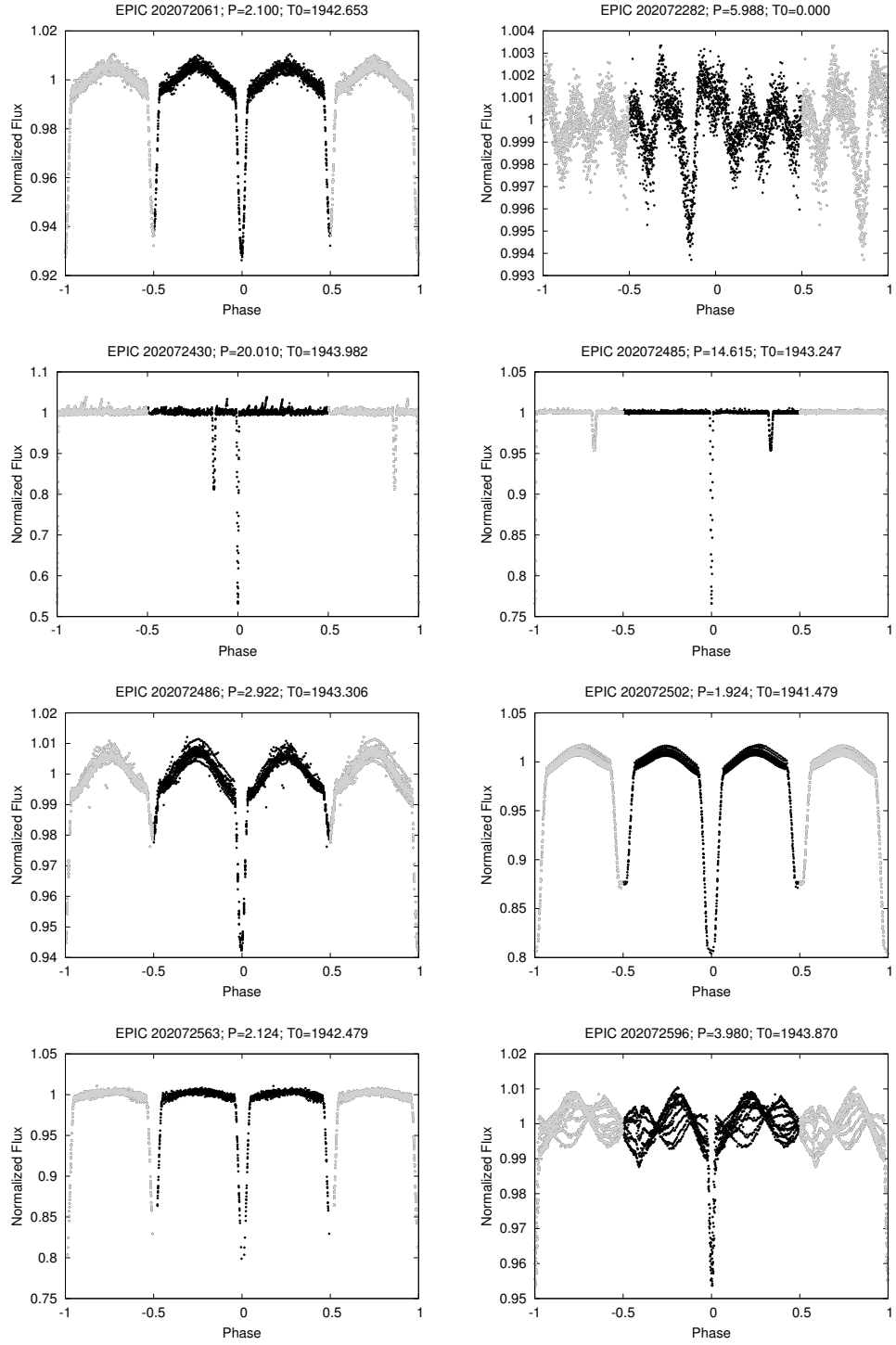


Fig. 5.— Plots of phased light curves for new eclipsing systems. Ephemerides are presented in Tables 2, 3, and 4. See Section 4 for details.

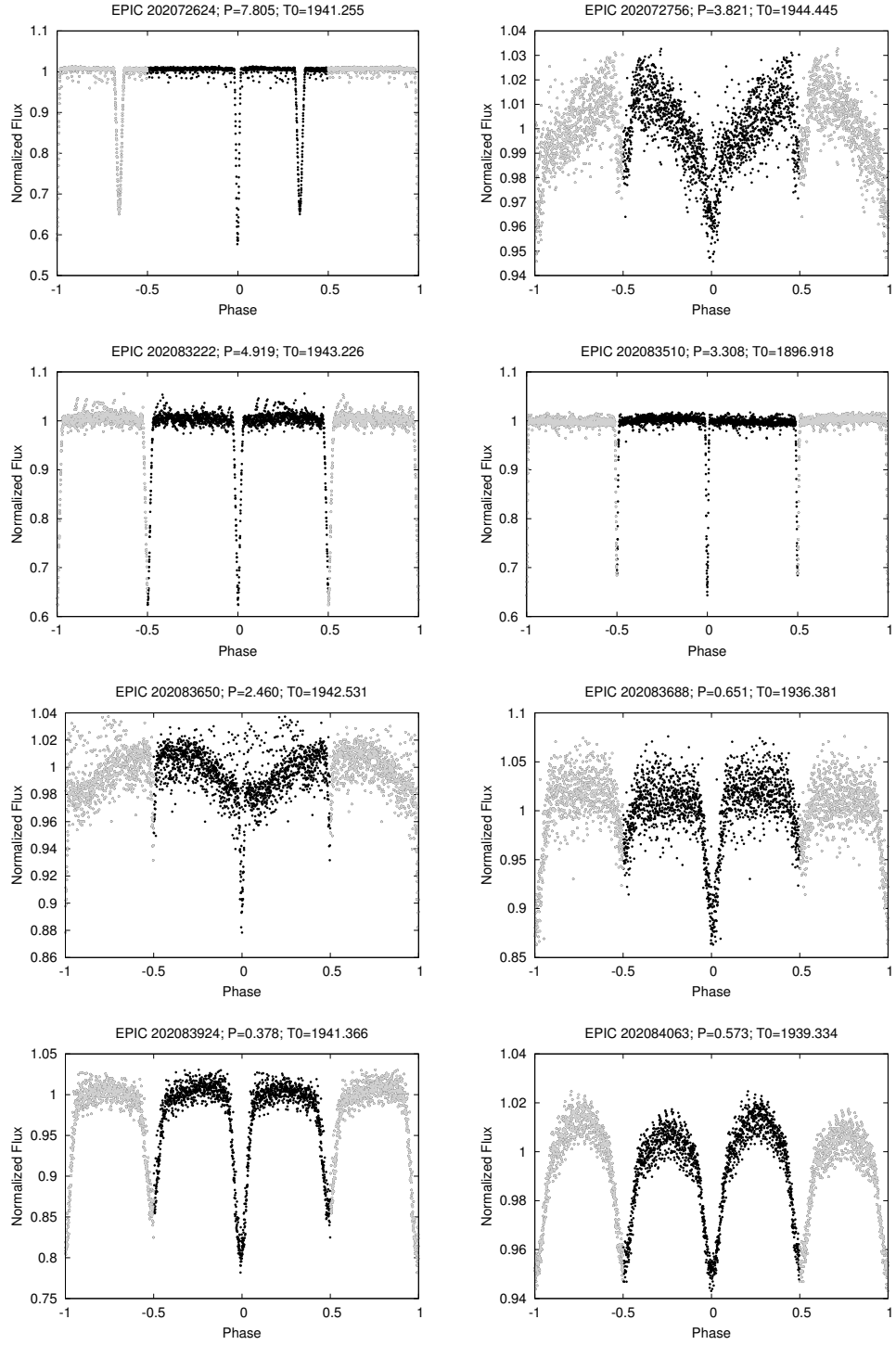


Fig. 6.— Plots of phased light curves for new eclipsing systems. Ephemerides are presented in Tables 2, 3, and 4. See Section 4 for details.

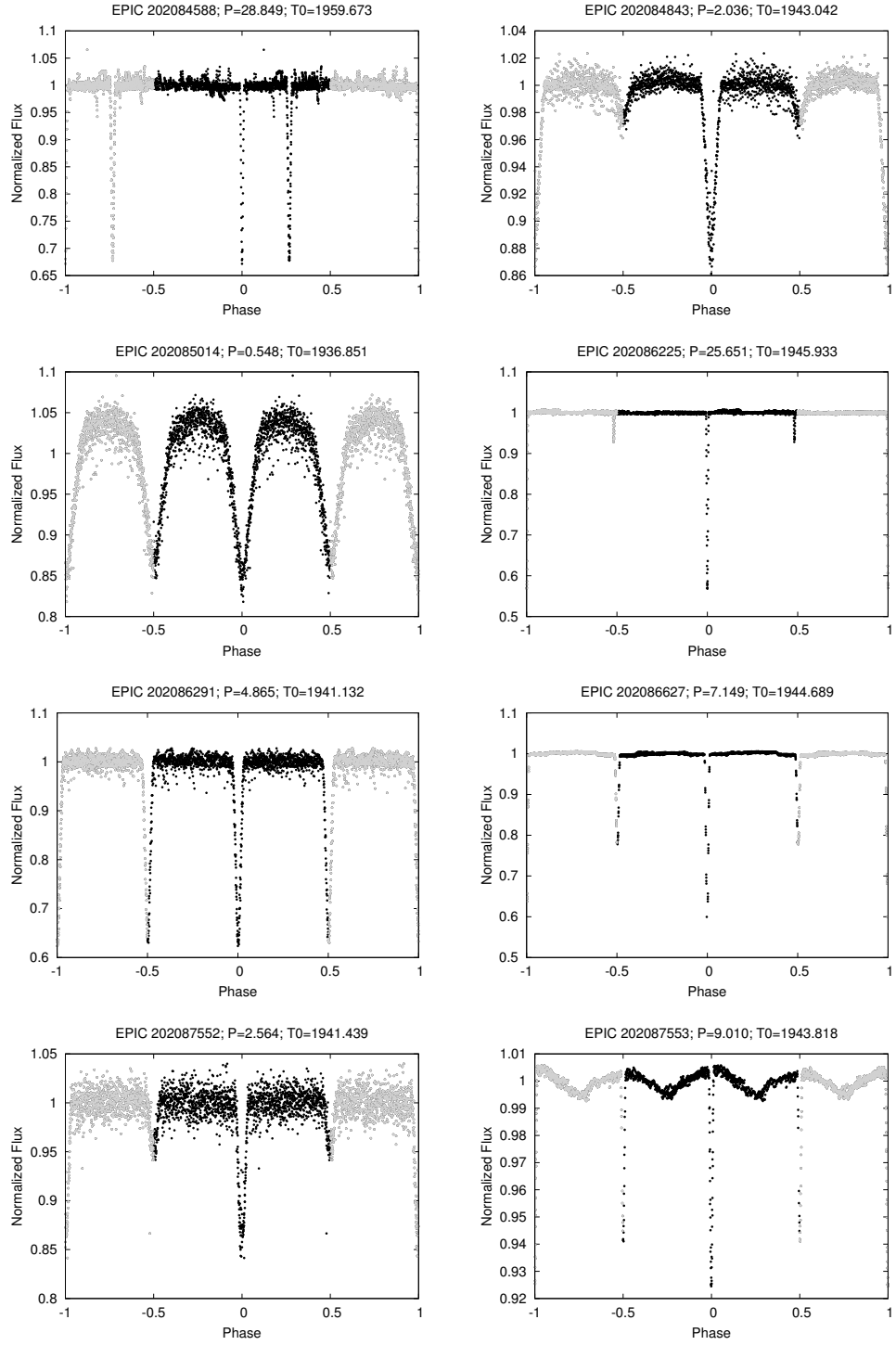


Fig. 7.— Plots of phased light curves for new eclipsing systems. Ephemerides are presented in Tables 2, 3, and 4. See Section 4 for details.

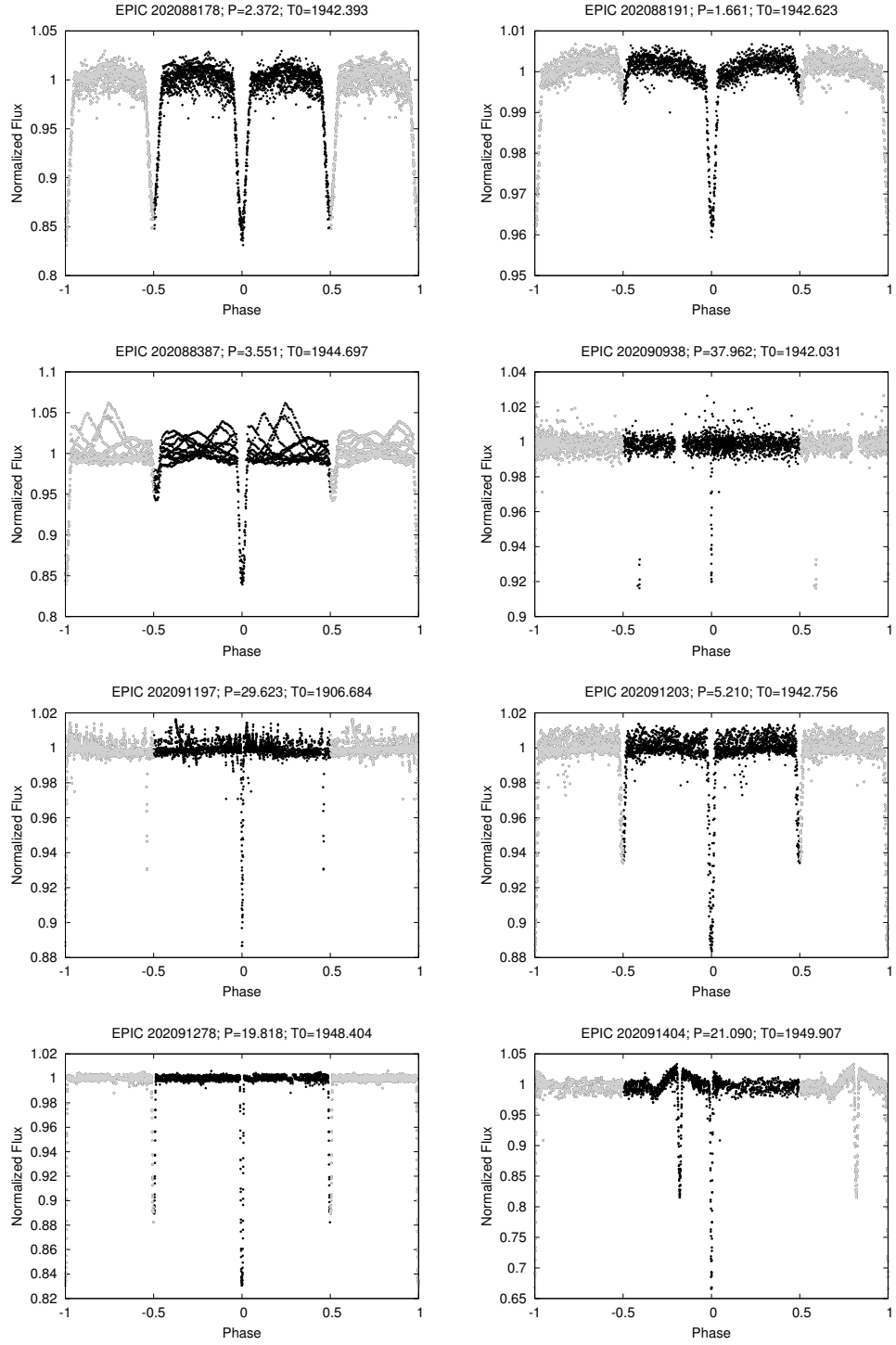


Fig. 8.— Plots of phased light curves for new eclipsing systems. Ephemerides are presented in Tables 2, 3, and 4. See Section 4 for details.

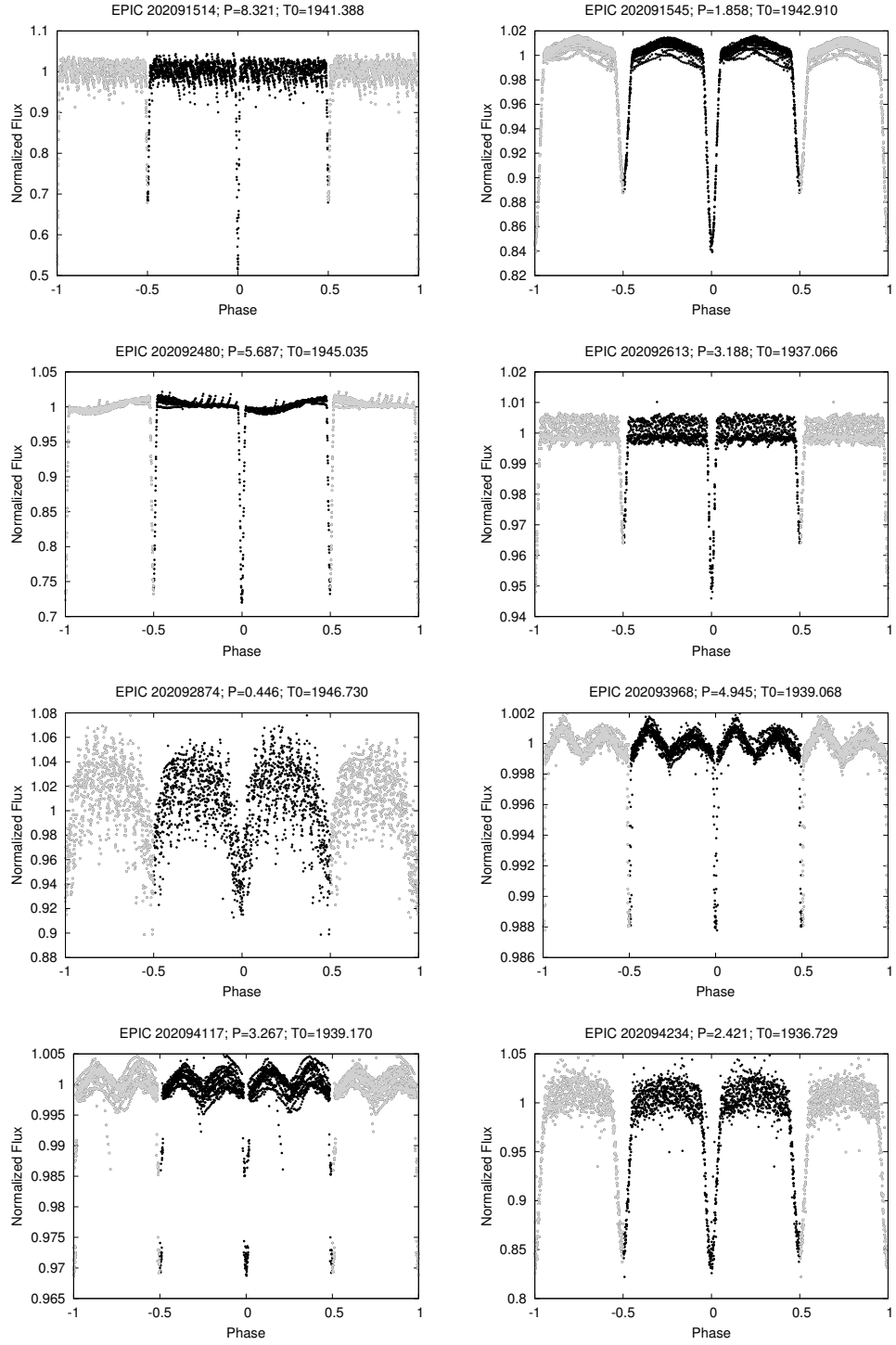


Fig. 9.— Plots of phased light curves for new eclipsing systems. Ephemerides are presented in Tables 2, 3, and 4. See Section 4 for details.

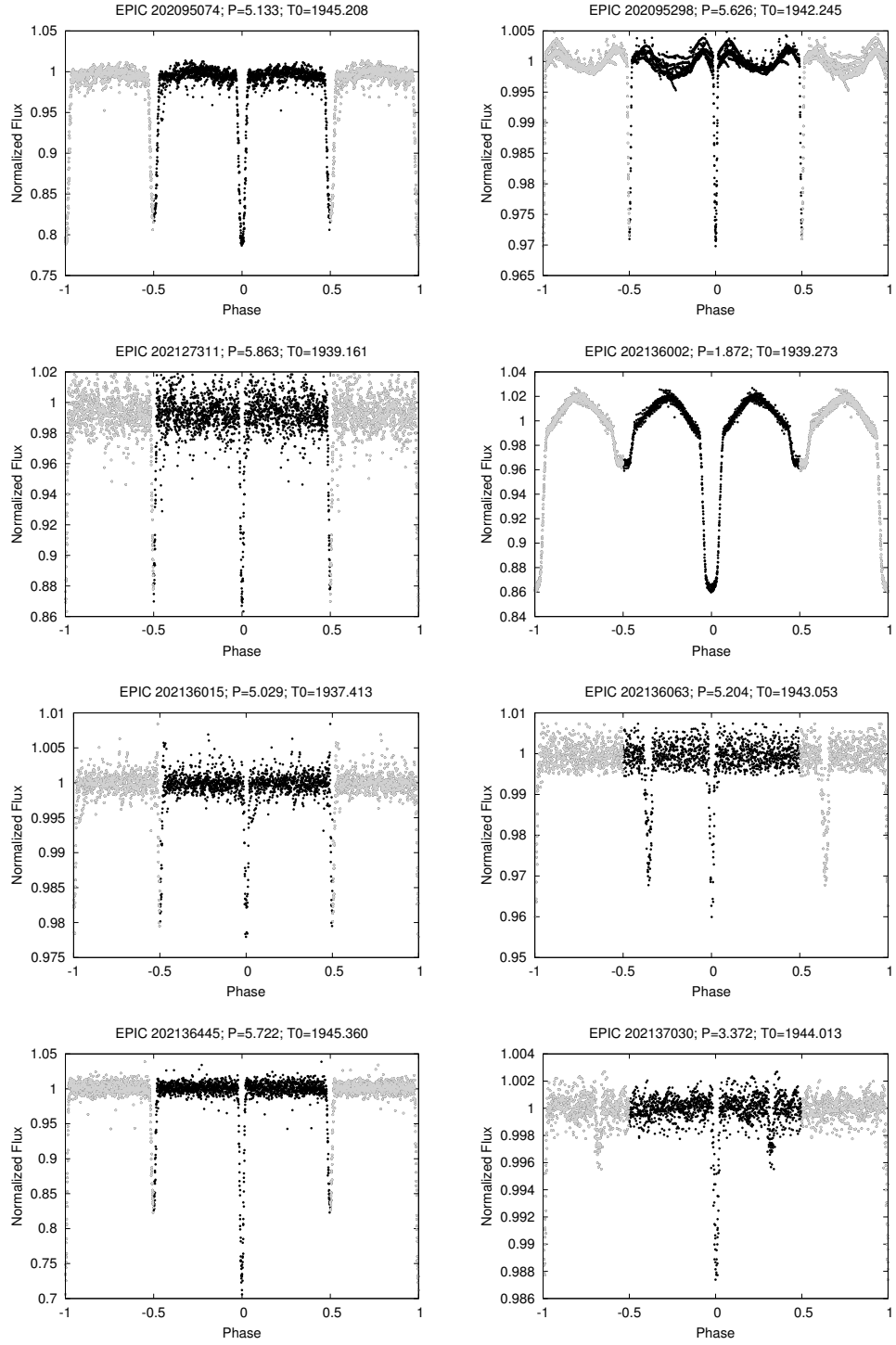


Fig. 10.— Plots of phased light curves for new eclipsing systems. Ephemerides are presented in Tables 2, 3, and 4. See Section 4 for details.

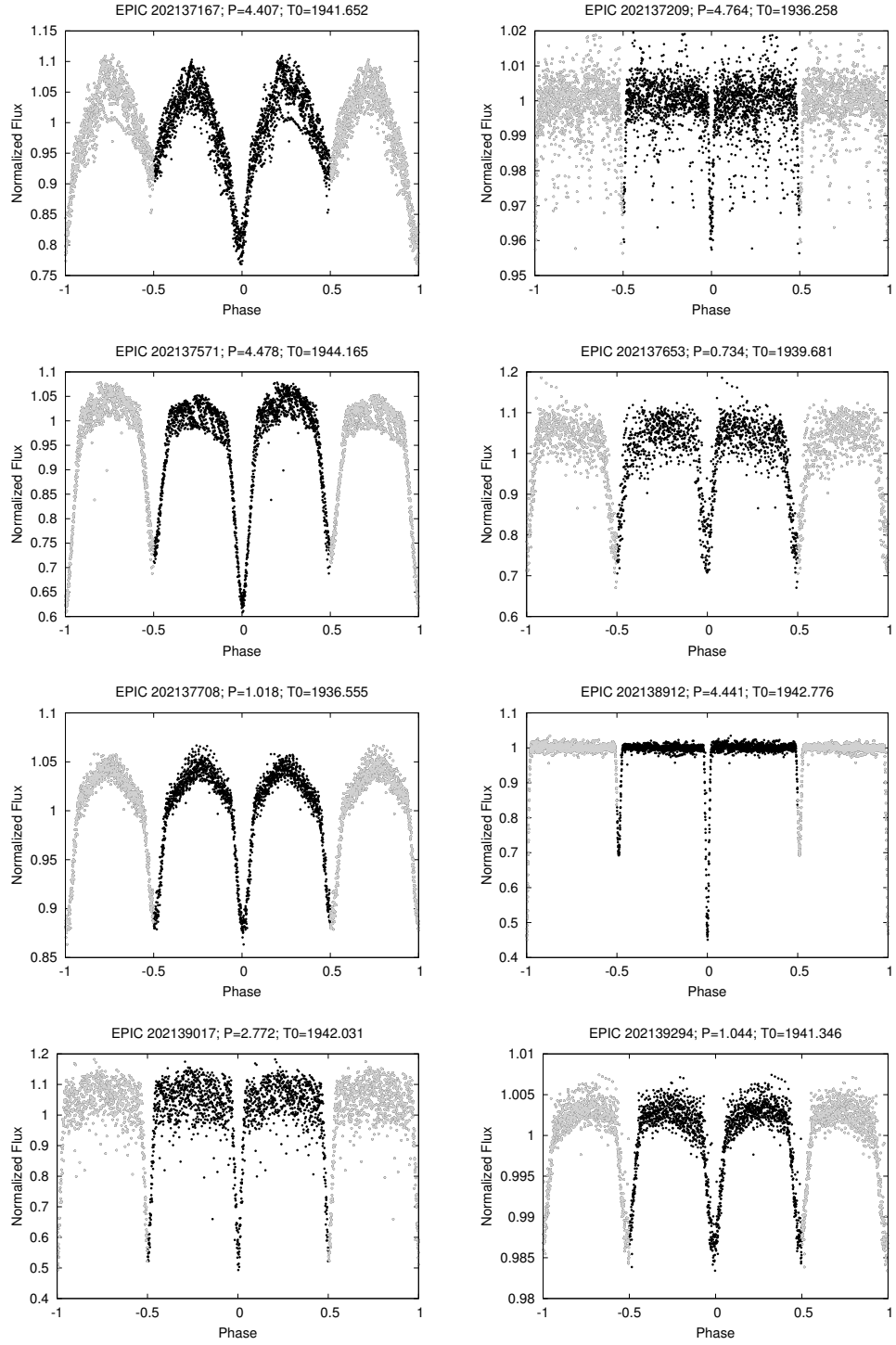


Fig. 11.— Plots of phased light curves for new eclipsing systems. Ephemerides are presented in Tables 2, 3, and 4. See Section 4 for details.

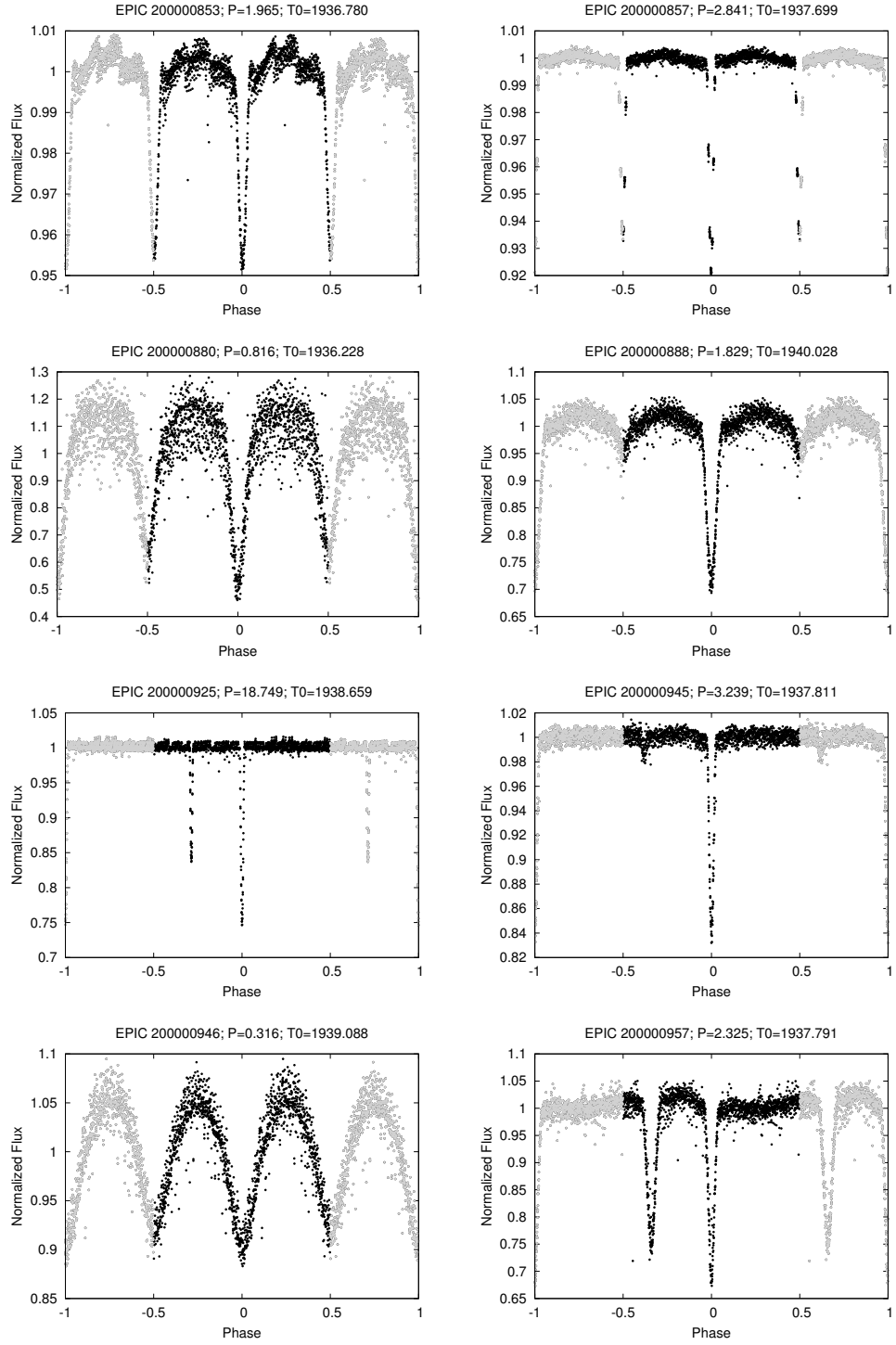


Fig. 12.— Plots of phased light curves for new eclipsing systems. Ephemerides are presented in Tables 2, 3, and 4. See Section 4 for details.

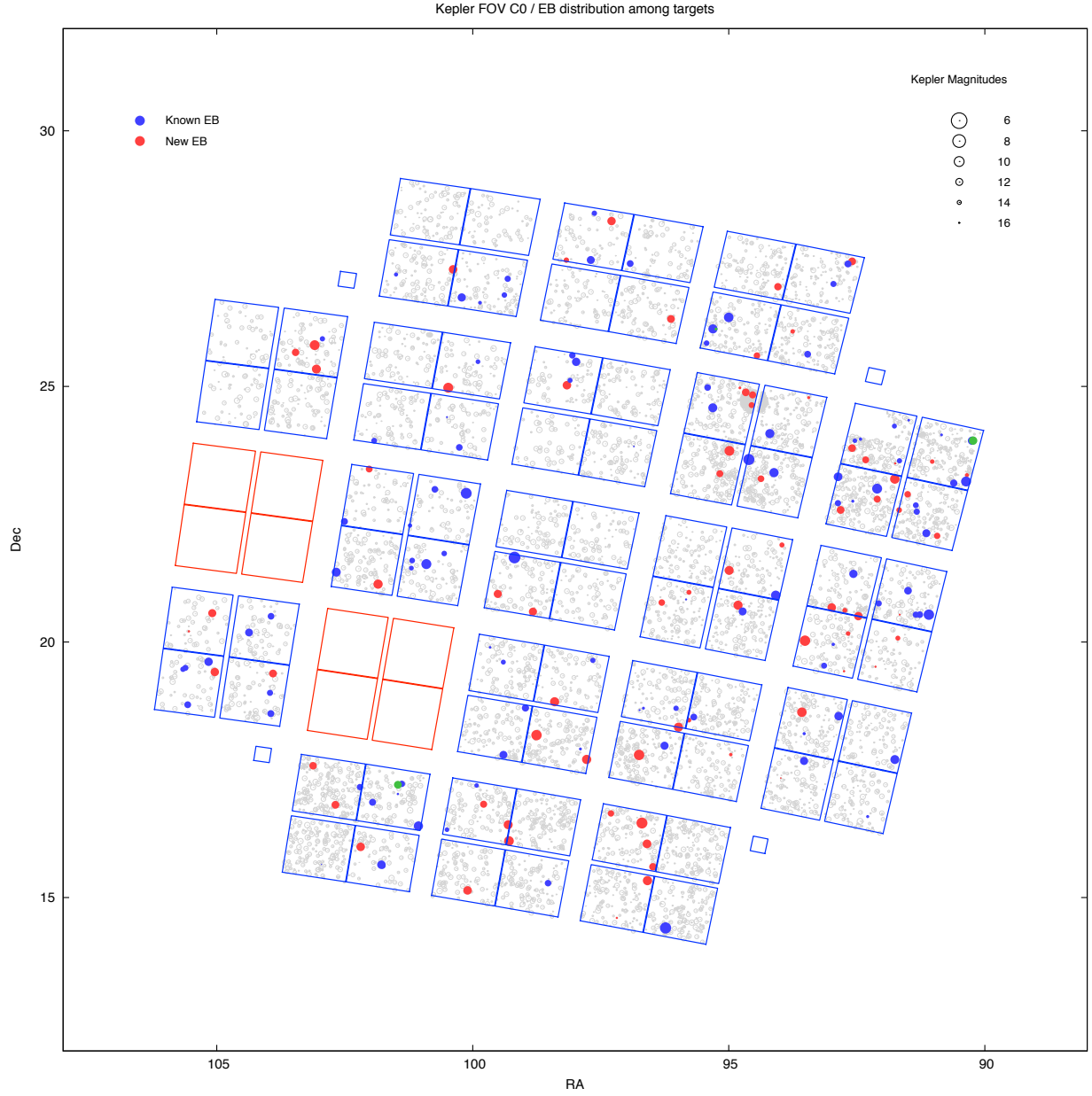


Fig. 13.— K2 C0 field of view with positions plotted for of all eclipsing systems listed in Table 1 (red), Table 2, and Table 4 (blue). Data point size corresponds to apparent K_p magnitude. The three green data points correspond to the two exoplanet candidates and suspected false positive described in Section 8.

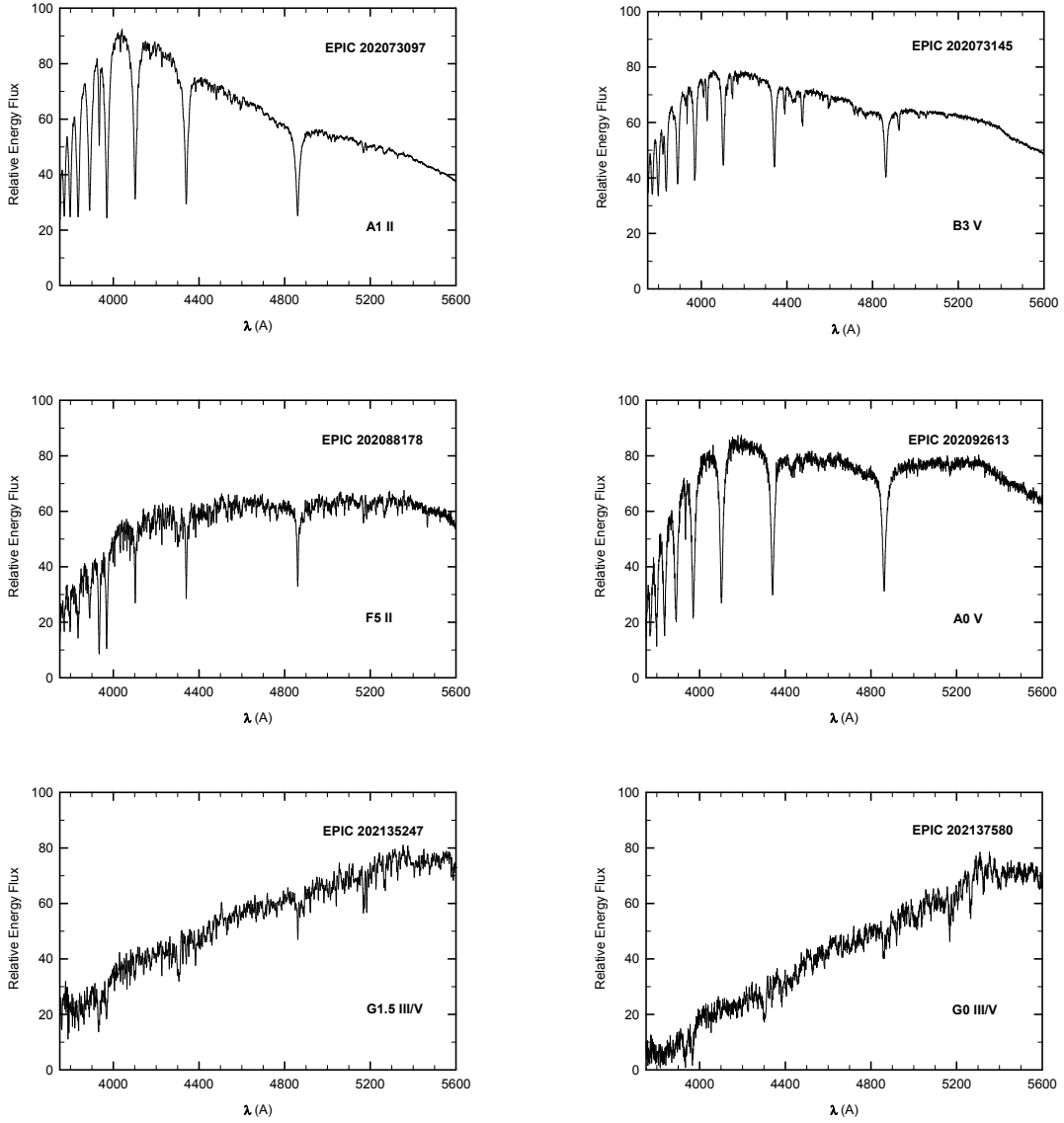


Fig. 14.— Spectra for selected EBs (EPIC 202073097, 202073145, 202088178, 202092613, 202135247, 202137580) described in Section 5 and 7. Spectral type for each object is given in the bottom right of each panel.

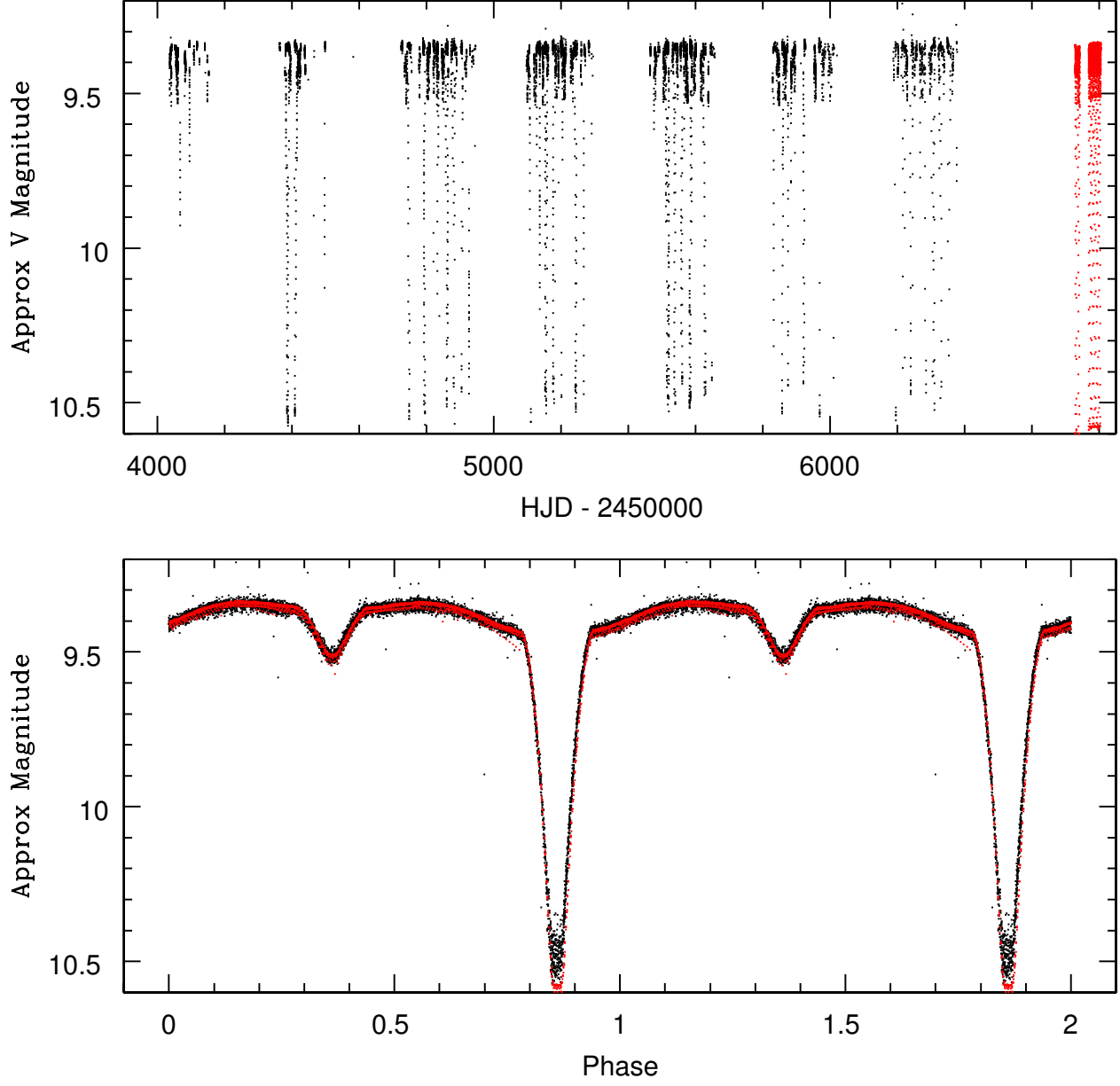


Fig. 15.— Light curves for EPIC 202060135 from data taken with KELT (black) and K2 (red). The top panel displays the full light curves, showing the full power of the 7-year baseline from KELT. The bottom panel shows the phased light curve. The KELT light curve appears slightly shallower than the K2 light curve in the primary eclipse due to the difference in bandpasses. For details, see Section 6.

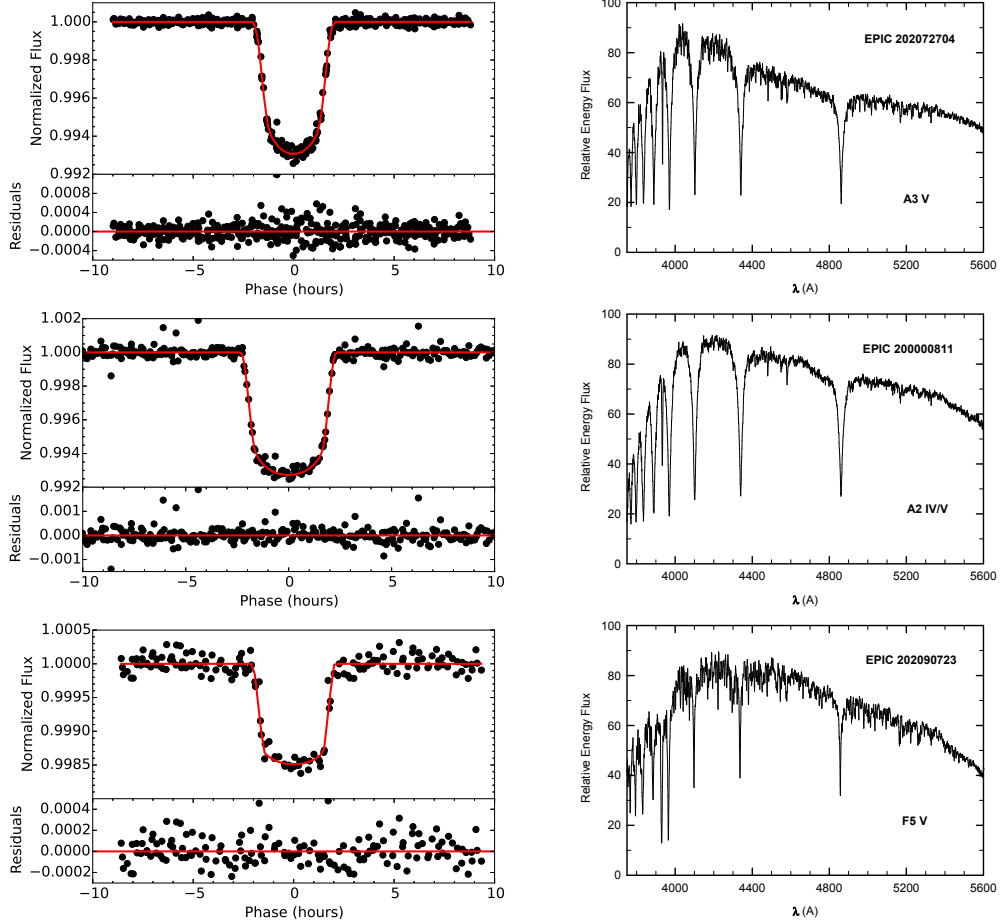


Fig. 16.— *Left column:* Phase-folded transit light curves with TAP model over plotted in red. *Right column:* The associated OMM spectrum of each star with the object’s spectral type in the bottom right of each panel. The top two rows are the planet candidates identified in this paper; the bottom row is EPIC 202090723, a likely false positive. See Section 8 for details.

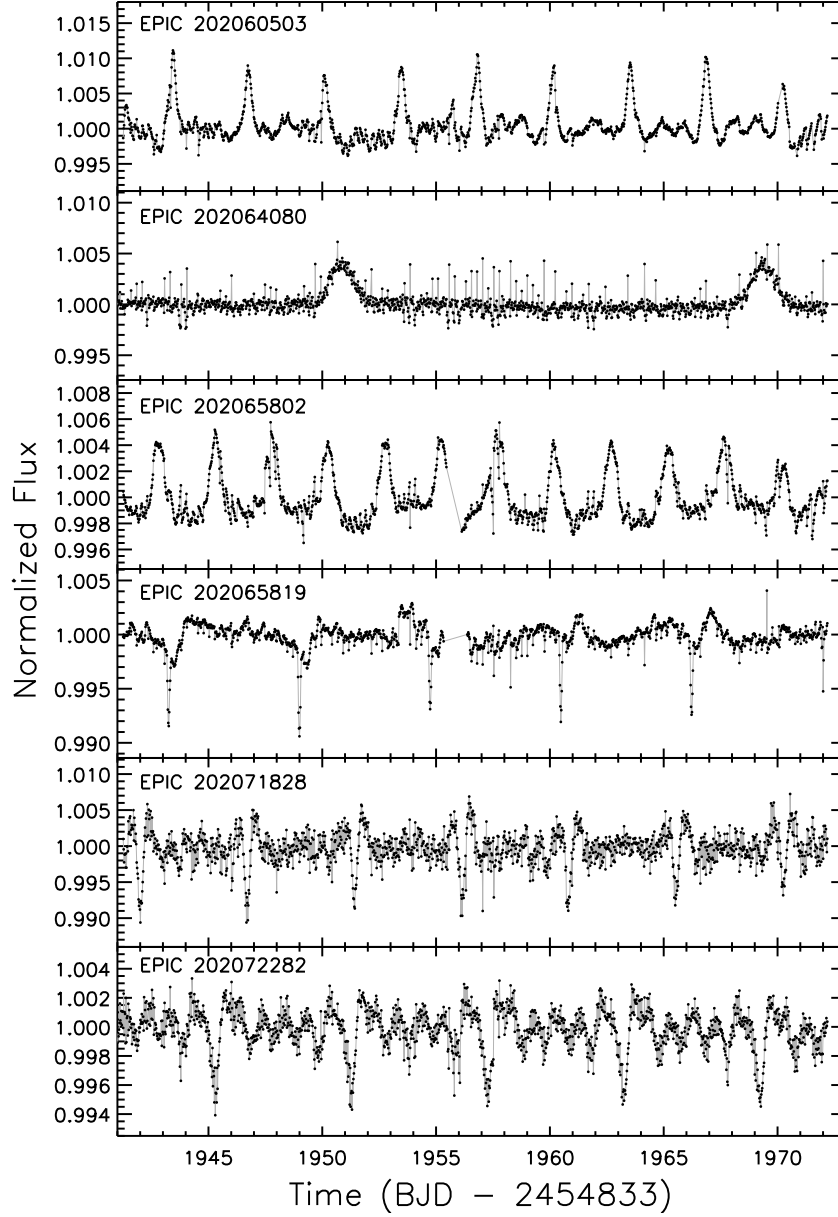


Fig. 17.— Light curves for six Heartbeat binaries detected in our C0 sample. See Section 7 and Table 2 for details.

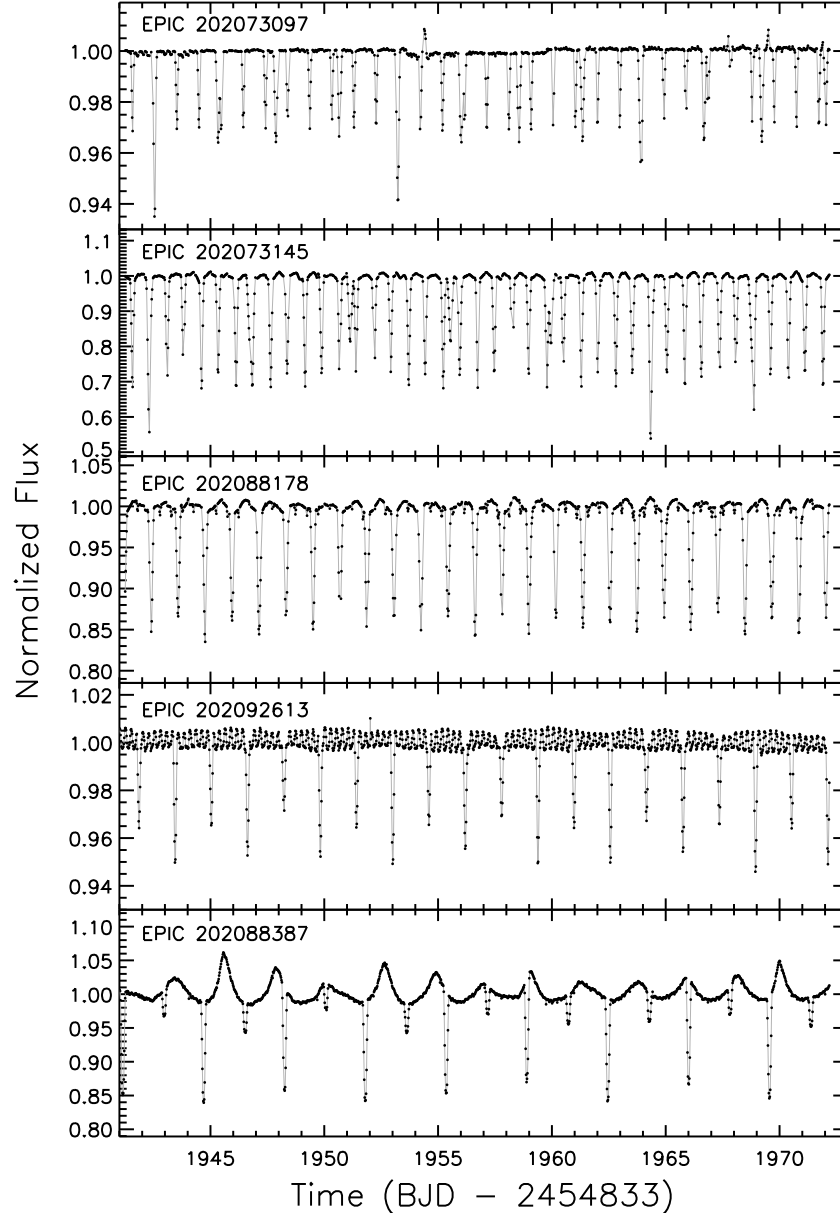


Fig. 18.— Full light curves for notable C0 EBs. From top to bottom: EPIC 202073097, 202073145, 202088178, 202092613, and 202088387. See Section 7 for details.

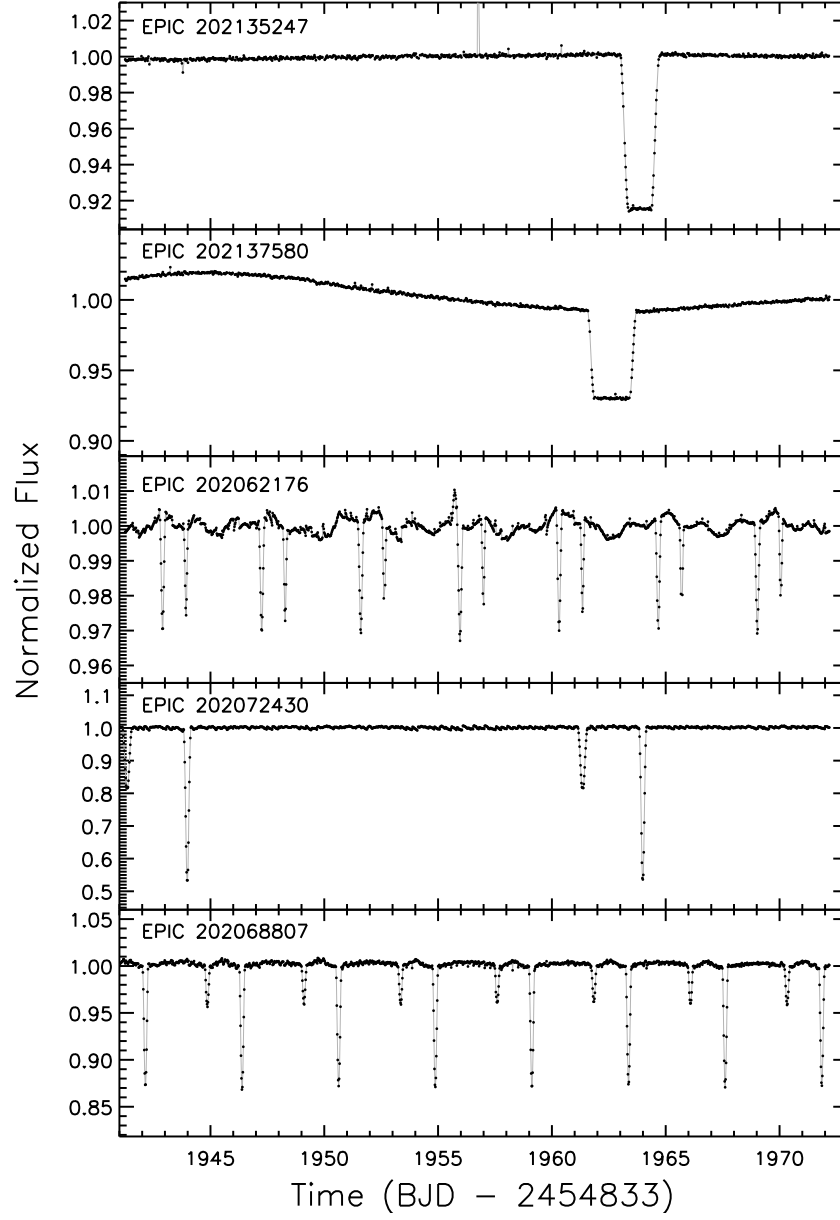


Fig. 19.— Full light curves for notable C0 EBs. From top to bottom: EPIC 202135247, 202137580, 202062176, 202072430, and 202068807. See Section 7 for details.

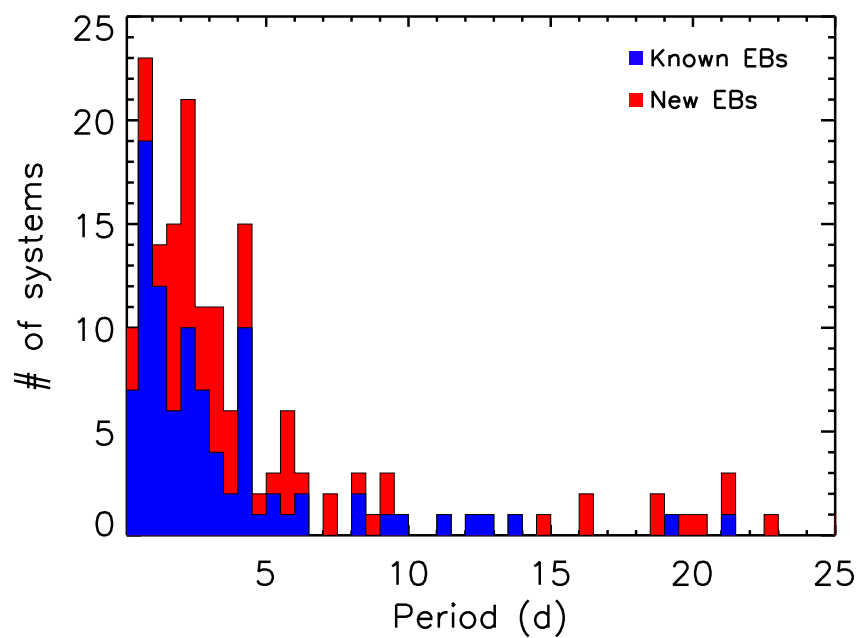


Fig. 20.— Period distribution for new and known K2 C0 eclipsing binaries with periods under 25 days.

Table 1. Previously Known EBs in Campaign 0

EPIC	K_P (mag)	RA (deg)	DEC (deg)	morph	Period (days)	BJD ₀ (BJD-2454833)	Cross matched identification	Note Flag
202059360	9.00	96.23357	14.40689	0.63	3.674801	1942.5111	CCDM J06249+1 (**); 2MASS 06245606+1424249	
202059377	8.70	99.18429	21.65157	0.55	1.576882	1942.7053	HD 46882 (Star); 2MASS 06364422+2139056	
202059416	9.70	102.71083	16.23806	0.59	0.900783	1941.6122	HD 264884 (Star); 2MASS 06505062+1614177	
202060124	9.10	94.60670	23.57145	0.65	4.285046	1943.0287	V* LT Gem (EB*); 2MASS 06182560+2334172	
202060135	9.89	90.36692	23.14098	0.55	2.865379	1943.2567	V* RW Gem (EB*Algol); 2MASS 06012805+2308274	
202060541	10.27	94.08259	20.91274	0.76	4.049160	1944.4214	HD 254205 (Star); 2MASS 06161955+2054502	
202060752	10.80	92.86670	23.23170	0.74	0.770391	1941.4077	ASAS J061128+2313.9; 2MASS 06112770+2313532	
202061814	13.40	91.76612	24.22436	0.82	1.021701	1941.9754	[GMB2010] WO (SB); 2MASS 06070387+2413277	
202062154	11.50	93.64370	18.47454	0.84	13.643500	1944.09	V* V2789 Ori (EB*betLyr); 2MASS 06143448+1828283	
202063828	10.60	102.66519	21.36553	0.57	1.243528	1943.1855	V* AF Gem (EB*Algol); 2MASS 06503974+2121596	
202064026	11.20	96.25542	17.97021	0.52	4.067909	1944.0496	V* BO Gem (EB*Algol); 2MASS 06250115+1758032	
202064535	11.30	97.69583	27.47333	0.80	0.508341	1941.5144	ASAS J063047+2728.4; 2MASS 06304688+2728258	
202064549	13.10	97.62533	28.38753	0.13	9.763444	1944.8127	2MASS 06302924+2823149	
202065543	10.40	101.06046	16.40108	0.59	1.446499	1941.5102	V* V382 Gem (EB*Algol); 2MASS 06441514+1623599	
202071266	12.50	91.33042	22.54782	0.78	2.593621	1944.18	V* DS Gem (Orion_V*); 2MASS 06051954+2232527	
202071842	9.90	100.90493	21.52375	0.30	4.168098	1943.0289	TYC 1342-1581-1 (Star); 2MASS 06433718+2131255	
202072451	11.30	99.40000	17.79239	0.25	11.306934	1949.92	V0400 Gem (EB*Algol); 2MASS 06373603+1747326	
202072929	10.50	97.98333	19.66989	0.50	3.05	1943.20	V* AY Gem (EB*Algol); 2MASS 06315619+1940115	
202072932	10.50	95.30965	26.12376	0.39	3.133688	1941.5201	TYC 1882-433-1 (Star); 2MASS 06211420+2607209	
202072933	12.20	100.73799	22.98607	0.06	3.144429	1944.0016	2MASS 06425680+2259128	
202072941	14.80	96.66667	18.70383	0.54	12.447767	1950.07	V* DU Gem (EB*Algol); 2MASS 06263978+1842228	
202072958	10.50	94.19764	24.07841	0.50	4.024547	1942.6683	TYC 1878-1258-1 (Star); 2MASS 06164724+2404389	
202072961	9.30	100.12564	22.91052	0.40	4.097024	1945.3702	HD 261572 (Star); 2MASS 06402979+2254445	
202072963	11.40	104.37154	20.18725	0.41	4.209922	1941.5103	TYC 1352-1219-1 (Star); 2MASS 06572939+2011151	
202072971	15.50	96.74292	18.66639	0.58	4.399157	1944.2988	V* DV Gem (EB*Algol); 2MASS 06265777+1839547	
202072978	12.20	100.26213	23.80780	0.54	4.885995	1944.6566	CCDM J06410+2 (*in**); 2MASS 06410235+2348198	
202072988	10.60	91.75583	17.70056	0.52	5.322461	1946.1201	V* CP Ori (EB*Algol); 2MASS 06070185+1741581	
202072991	10.20	95.00300	26.34982	0.47	5.495907	1945.3442	V* V396 Gem (EB*Algol); 2MASS 06200072+2620593	
202073004	15.20	101.46042	17.02611	0.57	6.154338	1946.518	V* KU Gem (EB*Algol); 2MASS 06455049+1701347	
202073035	12.20	103.93750	20.50333	0.83	21.4100	1945.59	ASAS J065545+2030.2; 2MASS 06554469+2030131	
202073040	12.20	91.27080	20.53500	0.55	2.121410	1941.4715	TYC 1321-16-1 (Star); 2MASS 06050489+2032128	
202073043	13.70	99.92500	17.19211	...	52.266500	1949.445	V* EU Gem (EB*Algol); 2MASS 06394202+1711355	2
202073061	14.60	93.52667	18.20556	0.06	2.482188	1943.79	V* V644 Ori (EB*Algol); 2MASS 06140639+1812098	
202073063	11.50	91.50028	21.00122	0.45	2.412447	1942.85	TYC 1325-414-1 (Star); 2MASS 06055967+2100001	

Table 1—Continued

EPIC	K_P (mag)	RA (deg)	DEC (deg)	morph	Period (days)	BJD ₀ (BJD-2454833)	Cross matched identification	Note Flag
202073067	13.80	101.22500	22.27639	0.61	2.349227	1943.206	V* IP Gem (EB*betLyr); 2MASS 06445396+2216348	
202073068	12.80	91.34558	22.67711	0.58	2.334819	1942.5926	TYC 1864-1836-1 (Candidate_EB*); 2MASS 06052293+2240375	
202073074	12.50	91.34580	20.53500	0.54	2.243308	1942.6813	2MASS 06052247+2032120	
202073088	14.50	92.96083	19.95389	0.57	0.824149	1941.3464	V* V668 Ori (EB*Algol); 2MASS 06115063+1957141	
202073096	11.80	98.97030	18.70835	0.93	1.960230	1942.4908	TYC 1333-46-1 (Star); 2MASS 06355255+1842337	
202073097	9.60	91.09233	20.53502	0.36	0.972411	1941.9621	HD 251042 (Star); 2MASS 06042191+2032032	3
202073117	12.70	93.13750	19.53667	0.59	1.762277	1942.9571	NSVS 9739376 (Candidate_EB*); 2MASS 06123367+1932132	
202073121	15.70	96.85250	23.82528	0.52	4.201499	1944.51	V* HU Gem(EB*Algol); 2MASS 06272454+2349310	
202073124	13.40	99.40333	19.60750	0.55	1.677702	1941.5202	V* TZ Gem (EB*Algol); 2MASS 06373732+1936236	
202073144	11.10	100.21498	26.74048	0.56	1.550610	1941.7757	TYC 1888-310-1 (Star); 2MASS 06405105+2644286	
202073145	11.30	94.72917	20.59833	0.54	1.516638	1942.2704	TYC 1323-169-1 (Star); 2MASS 06185463+2036038	3
202073160	13.20	97.65417	19.64122	0.57	1.412923	1942.47	V* CK Gem (EB*Algol); 2MASS 06303710+1938280	
202073161	14.80	97.89708	17.90667	0.54	1.403637	1942.3089	V* CM Gem (EB*betLyr); 2MASS 06313532+1754237	
202073174	12.00	103.94292	18.59806	0.65	1.288439	1941.7416	TYC 1335-728-1 (Star); 2MASS 06554632+1835554	
202073175	12.60	92.07080	20.75330	0.54	1.281167	1941.8027	ASAS J060817+2045.2; 2MASS 06081675+2045150	
202073185	13.10	96.02920	18.70330	0.62	0.612481	1941.7653	V* GZ Gem (EB*Algol); 2MASS 06240682+1842112	
202073186	10.40	94.11483	23.31200	0.55	1.224829	1941.7959	CCDM J06165+2 (*IN**); 2MASS 06162816+2318506	
202073203	12.90	101.18333	21.59333	0.61	1.198015	1942.501	ASAS J064444+2135.6; 2MASS 06444368+2135371	
202073207	14.70	92.57667	22.75333	0.58	1.050329	1942.2679	V* BS Gem (EB*Algol); 2MASS 06101841+2245114	
202073210	14.70	92.28667	16.58583	0.53	1.025071	1942.05	V* V667 Ori (EB*betLyr); 2MASS 06090828+1635064	
202073217	12.40	101.38521	17.22515	0.60	0.941135	1941.319	V* EY Gem (EB*betLyr); 2MASS 06453218+1713361	
202073218	13.00	100.55833	21.73000	0.64	0.921221	1941.4036	ASAS J064214+2143.8; 2MASS 06421396+2143506	
202073232	12.30	98.52917	15.28167	0.80	0.838008	1941.667	ASAS J063407+1516.9; 2MASS 06340720+1516541	
202073235	12.00	101.95687	16.86322	0.60	0.819121	1941.4962	V* FG Gem (EB*Algol); 2MASS 06474902+1651469	
202073238	11.80	90.60747	23.10947	0.64	0.791658	1941.5186	ASAS J060226+2306.5; 2MASS 06022579+2306340	
202073248	12.80	101.92500	23.93661	0.65	0.757302	1941.69	V* V383 Gem (EB*Algol); 2MASS 06474171+2356022	
202073253	11.20	93.53042	17.67444	0.74	0.733801	1941.62	ASAS J061407+1740.5 (Candidate_EB*); 2MASS 06140718+1740269	
202073262	14.90	90.84625	24.05083	0.59	2.246169	1942.6555	V* DR Gem (EB*WUMa); 2MASS 06032303+2403028	
202073266	12.10	96.92732	27.40250	0.94	0.689607	1941.9902	TYC 1887-1247-1 (Star); 2MASS 06274249+2724083	
202073267	12.50	92.86917	22.71556	0.62	0.684031	1941.52	ASAS J061129+2242.9 (Star); 2MASS 06112855+2242578	
202073270	10.90	92.85417	18.54989	0.62	0.659306	1941.4588	V* V392 Ori (EB*Algol); 2MASS 06112516+1832596	
202073276	12.00	102.50708	22.35778	0.76	0.644164	1941.66	ASAS J065002+2221.5 (Candidate_EB*); 2MASS 06500165+2221277	
202073297	15.40	95.83333	20.83286	0.62	0.527435	1941.46	V* GR Gem (EB*betLyr); 2MASS 06232025+2049578	
202073307	12.60	92.95463	27.00535	0.72	0.505216	1941.7346	2MASS 06114893+2700259	

Table 1—Continued

EPIC	K_P (mag)	RA (deg)	DEC (deg)	morph	Period (days)	BJD ₀ (BJD-2454833)	Cross matched identification	Note Flag
202073319	10.90	101.78330	15.64330	0.76	0.462071	1941.4898	V* V405 Gem (EB*WUMa); 2MASS 06470785+1538369	
202073346	12.50	99.31727	27.10678	0.75	0.384243	1941.459	TYC 1888-1317-1 (Star); 2MASS 06371598+2706167	
202073348	12.10	93.46083	25.62861	0.77	0.320736	1942.9913	ASAS J061351+2537.7 (Candidate_EB*); 2MASS 06135085+2537402	
202073353	12.00	92.67190	27.39488	0.77	0.371250	1941.5099	2MASS 06104125+2723415	
202073361	11.10	90.25184	23.93759	0.75	0.361833	1941.41	TYC 1864-1065-1 (Candidate EB*); 2MASS 06010044+2356153	
202073397	12.60	103.95833	19.00333	0.94	0.345527	1941.3673	ASAS J065550+1900.2; 2MASS 06555020+1900166	
202073438	15.00	99.66250	19.89447	0.52	2.405896	1943.0241	V* OQ Gem (EB*Algol); 2MASS 06383922+1953397	
202073440	13.20	91.66625	23.54556	0.40	2.624142	1941.72	V* LQ Gem (EB*); 2MASS 06063990+2332435	
202073442	13.70	92.53767	23.93611	0.95	3.867399	1943.69	[GMB2010] WO (SB); 2MASS 06100903+2356099	
202073445	14.50	92.42750	23.96817	0.47	2.835402	1942.0075	[GMB2010] WO (SB); 2MASS 06094259+2358053	
202073476	15.00	91.48542	24.33889	0.34	...	1957.76	V* HN Gem (EB*Algol); 2MASS 06055652+2420201	1
202073489	12.60	101.76169	15.62306	0.73	0.348725	1941.547	V* V404 Gem (EB*WUMa); 2MASS 06470269+1537288	
202073490	13.50	101.19833	21.44417	0.58	2.029235	1942.9043	V* OR Gem (EB*Algol); 2MASS 06444669+2126378	—
202073495	15.50	100.50292	24.39889	0.53	2.860568	1943.0098	V* KO Gem (EB*Algol); 2MASS 06420065+2423568	42
202083021	16.00	102.95375	15.64889	0.60	2.933567	1940.9997	V* KX Gem (EB*Algol); 2MASS 06514889+1538558	—
202087711	11.00	98.69724	18.87943	0.41	2.29	1942.495	TYC 1337-48-1; 2MASS 06344733+1852459	
202103762	13.20	102.93668	25.93092	0.48	1.326493	1941.4718	2MASS 06514459+2555550	
202122545	13.30	98.09915	25.11887	0.04	19.2700	1950.8918	2MASS 06322356+2507167	2
202126825	13.09	105.66026	19.46655	0.21	9.206803	1947.8098	2MASS 07023846+1927595	
202126847	12.42	102.20130	17.16191	0.24	8.342127	1945.2552	2MASS 06484823+1709502	
202126851	13.96	101.49694	27.18665	0.32	4.480119	1945.9267	2MASS 06455926+2711119	
202126864	12.65	105.61144	19.49339	0.28	6.187675	1946.1115	2MASS 07022674+1929362	
202126871	13.62	100.50464	16.32700	0.87	8.431037	1942.6508	2MASS 06420111+1619371	
202126877	11.02	97.98012	25.48210	0.02	...	1955.44	TYC 1883-1721-1 (Star); 2MASS 06315522+2528555	1
202126878	12.25	95.41234	24.97781	0.29	5.559292	1946.2296	TYC 1882-1294-1 (Star); 2MASS 06213896+2458401	
202126880	12.96	95.43424	25.84569	0.29	3.460849	1941.51	2MASS 06214421+2550444; SDSS J062144.21+255044.4	
202126886	14.25	99.85710	26.63629	0.45	2.941136	1942.2333	2MASS 06392557+2638008	
202126887	13.03	99.38054	26.78655	0.07	12.85570	1944.2557	2MASS 06373133+2647115	

Note. — Table flags are as follows: 1) Single eclipse observed in C0, 2) Two primary eclipses observed in C0 (period unconfirmed), 3) Stellar T_{eff} estimated from OMM observation (Section 5)

Table 2. New EPIC EBs in K2 Campaign 0

EPIC	K_P (mag)	RA (deg)	DEC (deg)	morph	Period (days)	BJD ₀ (BJD-2454833)	Cross matched identification	Note flag
202060506	13.69	91.02725	23.52939	0.56	1.959777	1942.7863	2MASS 06040653+2331457; SDSS J060406.54+233145.7	
202060523	10.20	94.98682	23.73928	0.13	16.409028	1946.9955	HD 255133; 2MASS 06195683+2344214	
202060551	10.35	91.75614	23.18982	0.17	16.496998	1946.2014	HD 251696; 2MASS 06070147+2311234	
202060577	10.5	93.07996	25.58141	0.60	1.019488	1939.4459	2MASS 06121919+2534530	
202060800	11.58	92.59105	23.79414	0.31	3.262032	1940.6815	HD 252612; 2MASS 06102186+2347390	
202060911	12.60	92.10217	22.79439	0.31	7.024977	1945.8409	GSC 01877-0048; 2MASS 06082451+2247398	
202060921	12.00	92.32424	23.56279	0.03	...	1971.3295	TYC 1877-964-1; 2MASS 06091781+2333462	1
202061000	12.40	90.93004	22.07661	0.36	5.869057	1943.0212	GSC 01325-0100; 2MASS 06034320+2204357	
202062176	11.00	92.46929	20.50456	0.36	4.354250	1942.8988	2MASS 06095262+2030273	
202063160	9.30	96.69498	16.45886	0.45	9.069795	1943.0525	HD 45193; 2MASS 06264647+1627422	
202064080	11.40	92.81720	22.58563	...	18.6700	1950.8607	HD 252893; 2MASS 06111653+2235072	3
202064253	12.30	91.50423	22.89176	0.06	21.1403	1944.993	TYC 1864-1626-1; 2MASS 06060100+2253303	
202065802	11.53	94.66820	24.88376	...	2.488563	1942.8072	2MASS 06184036+2453015; SDSS J061840.14+245257.0	3
202065819	11.90	94.53534	24.83398	...	5.744089	1943.2566	2MASS 06180848+2450023; SDSS J061808.48+245002.2	3
202066394	14.30	95.43298	25.03245	0.34	3.186362	1941.7972	2MASS 06214391+2501569; SDSS J062143.91+250156.8	
202066699	14.40	98.24756	26.86962	0.50	2.215812	1942.0412	2MASS 06325941+2652106; SDSS J063259.41+265210.6	
202066811	14.50	103.36132	16.83309	0.54	1.696599	1942.2817	2MASS 06532672+1649592	
202068686	12.21	94.37093	23.19523	0.17	8.753366	1947.1591	TYC 1878-625-1; 2MASS 06172901+2311431	
202068807	12.02	95.17472	23.29332	0.35	4.244843	1942.1365	TYC 1878-947-1; 2MASS 06204185+2317264	
202071293	10.80	96.59682	16.05121	0.68	0.572925	1941.6329	2MASS 06262323+1603043	
202071505	10.10	99.29125	16.10936	0.31	3.555458	1942.7771	TYC 1329-1160-1; 2MASS 06370987+1606445	
202071579	10.40	96.58702	15.33108	0.43	3.127251	1941.4203	TYC 1328-1566-1; 2MASS 06262107+1519429	
202071631	10.50	98.40078	18.83125	0.58	3.473756	1937.0563	TYC 1337-314-1; 2MASS 06333619+1849524	
202071635	10.20	93.57181	18.62702	0.20	6.270290	1942.4393	TYC 1318-530-1; 2MASS 06141723+1837373	
202071731	10.60	99.30961	16.42521	0.51	2.740255	1942.0820	TYC 1329-456-1; 2MASS 06371430+1625307	
202071828	10.90	98.16272	25.02194	...	4.708328	1942.0007	TYC 1883-2053-1; 2MASS 06323905+2501189	3
202071902	10.40	101.84678	21.13419	0.01	...	1958.5707	TYC 1342-1936-1; 2MASS 06472322+2108030	1
202071945	9.60	93.50981	20.02771	...	22.920600	1956.1625	BD+20 1321; 2MASS 06140273+2001306	2
202071994	9.60	96.75253	17.78967	0.43	4.051073	1945.0441	TYC 1332-561-1; 2MASS 06270059+1747227	
202072061	9.90	100.47882	24.97612	...	2.100424	1942.6534	TYC 1897-1168-1; 2MASS 06415491+2458339	
202072282	10.60	94.99049	21.40122	...	5.977524	1939.3031	TYC 1327-1570-1; 2MASS 06195750+2123545	3
202072430	10.90	100.10215	15.14237	0.11	20.007618	1943.9820	TYC 1330-2152-1; 2MASS 06402451+1508324	
202072485	10.90	102.18925	15.99120	0.09	14.6300	1943.2469	TYC 1331-1925-1; 2MASS 06484542+1559283	
202072486	11.20	105.08763	20.56381	0.49	2.921628	1943.3058	TYC 1352-289-1; 2MASS 07002042+2033458	

Table 2—Continued

EPIC	K_P (mag)	RA (deg)	DEC (deg)	morph	Period (days)	BJD ₀ (BJD-2454833)	Cross matched identification	Note flag
202072502	11.20	98.82478	20.59244	0.58	1.923701	1941.4794	TYC 1337-283-1; 2MASS 06351795+2035328	
202072563	11.00	105.03774	19.41262	0.50	2.123748	1942.4788	TYC 1352-1558-1; 2MASS 07000906+1924455	
202072596	11.20	99.51074	20.93931	0.35	3.979679	1943.87	TYC 1341-702-1; 2MASS 06380257+2056215	
202072917	11.90	99.78832	16.82623	0.02	...	1953.6261	TYC 1329-752-1; 2MASS 06390919+1649345	1
202083510	16.50	105.54264	20.20912	0.17	3.307592	1943.22	2MASS 07021029+2012333	
202083650	15.80	93.98480	17.33772	0.40	2.460416	1942.5311	2MASS 06155635+1720157	
202083924	14.00	90.35016	23.26361	0.58	0.378380	1941.3662	2MASS 06012405+2315497; SDSS J060124.07+231548.8	
202084588	15.30	92.13496	19.51602	...	28.78800	1959.6731	2MASS 06083199+1930591	2
202085014	14.70	93.43762	24.77931	0.65	0.547850	1936.8511	2MASS 06134502+2446455; SDSS J061345.04+244645.7	
202086225	12.30	96.30833	20.77100	...	25.6485	1945.9332	2MASS 06251404+2046206	2
202086291	12.30	94.44968	25.60257	0.54	2.434963	1943.563	2MASS 06174792+2536092; SDSS J061747.92+253609.1	
202086627	11.70	96.48285	15.60354	0.19	7.151257	1944.6892	2MASS 06255588+1536127	
202087553	13.70	92.66988	20.16510	0.23	9.001198	1943.8183	2MASS 06104077+2009543	
202088178	13.60	95.77925	18.47082	0.53	2.370616	1942.3929	2MASS 06230702+1828149	4
202088191	11.70	94.03926	26.95089	0.44	1.661616	1942.623	TYC 1885-208-1; 2MASS 06160906+2656555	
202088387	12.90	91.67373	22.58188	0.41	3.550170	1944.6967	2MASS 06064169+2234547; SDSS J060641.69+223454.8	
202091197	11.60	103.11794	17.57922	...	29.62270	1950.01	TYC 1335-1000-1; 2MASS 06522830+1734451	2
202091203	15.20	92.75029	19.42760	0.34	5.214161	1942.7558	2MASS 06110014+1925298	
202091278	11.70	103.45979	25.66458	0.18	19.8183	1948.4041	TYC 1898-2293-1; 2MASS 06535034+2539524	2
202091404	9.60	98.75453	18.17719	0.11	21.0842	1949.9074	TYC 1333-449-1; 2MASS 06350172+1810345	2
202091514	10.00	103.08750	25.80658	0.20	8.312728	1941.3878	TYC 1898-2911-1; 2MASS 06522100+2548236	
202091545	10.90	100.38259	27.28787	0.52	1.857788	1942.9097	TYC 1888-1789-1; 2MASS 06413182+2717163	
202092480	10.60	103.05227	25.33909	0.31	5.687839	1945.0349	TYC 1898-973-1; 2MASS 06521237+2520109	
202092613	13.30	93.96165	21.89863	0.37	3.187483	1943.44	2MASS 06155077+2154029	4
202092842	13.10	98.17189	27.47062	...	36.9350	1906.605	2MASS 06324125+2728142; SDSS J063241.25+272814.2	2
202093968	10.20	96.16126	21.12574	0.35	2.47000	1941.5364	CCDM J06246+2; 2MASS 06243870+2107326	
202094117	11.40	96.12867	26.31839	0.42	1.634486	1942.45	TYC 1886-455-1; 2MASS 06243088+2619061	
202094234	13.70	93.75359	26.07596	0.57	2.420777	1941.57	2MASS 06150153+2604278	
202095298	10.50	94.81912	20.72068	0.27	5.627027	1942.2452	TYC 1327-300-1; 2MASS 06191658+2043144	
202135247	14.40	94.96192	17.79667	0.26	...	1963.8686	2MASS 06195142+1747474	1,4
202137167	13.40	91.69799	20.07536	0.70	4.395594	1941.6524	2MASS 06064813+2004326	
202137209	15.50	91.66285	20.53502	0.47	2.381835	1936.2585	2MASS 06063908+2032060	
202137571	15.30	91.74892	23.49284	0.63	4.477240	1944.1655	2MASS 06065974+2329342; SDSS J060659.73+232934.3	
202137580	13.10	90.79350	23.50484	0.35	...	1962.645	2MASS 06031044+2330174	1,4

Table 2—Continued

EPIC	K_P (mag)	RA (deg)	DEC (deg)	morph	Period (days)	BJD ₀ (BJD-2454833)	Cross matched identification	Note flag
202139294	11.40	92.59146	27.44547	0.61	1.043312	1941.346	2MASS 06102194+2726436	

Note. — Table flags are as follows: 1) Single primary eclipse observed in C0, 2) Two primary eclipses observed in C0 (period unconfirmed), 3) Heartbeat binary candidate, 4) Stellar T_{eff} estimated from OMM observation (Section 5)

Table 3. M35 Superstamp EBs in Campaign 0^a

2MASS ID	K_P (mag)	RA (deg)	DEC (deg)	Period (days)	BJD ₀ (BJD-2454833)	Superstamp TPF	RA (deg)	Dec (deg)	Note Flag
2MASS 06081216+2431193	13.18	92.0504	24.5219	2.51	1937.11	200000819	92.0776	24.5320	2
2MASS 06093832+2417534	10.87	92.40956	24.29817	1.96	1936.7795	200000853	92.3814	24.3117	
2MASS 06083089+2415122	11.30	92.1285	24.25325	2.84	1937.6988	200000857	92.1450	24.2630	2
2MASS 06101142+24241552	14.51	92.5474	24.4044	0.81	1936.2278	200000880	92.5454	24.4019	2
2MASS 06094437+2434194	13.52	92.43516	24.57205	1.84	1937.28	200000884	92.4462	24.5513	
2MASS 06085327+2428371	12.99	92.2219	24.4771	1.82	1940.0357	200000888	92.2094	24.5027	
2MASS 06092044+2415155	16.31	92.3351	24.2544	0.52	1939.1598	200000924	92.3357	24.2457	2
2MASS 06090042+2414108	12.93	92.2516	24.2364	18.74	1938.6592	200000925	92.2766	24.2336	1
2MASS 06092929+2407028	16.30	92.3718	24.1176	0.39	1939.1086	200000940	92.3624	24.1380	2
2MASS 06101502+2408460	13.72	92.5623	24.1462	3.23	1937.8113	200000945	92.5528	24.1205	2
2MASS 06100186+2405498	13.43	92.5075	24.0972	0.31	1939.088	200000946	92.4938	24.1084	2
2MASS 06095723+2403294	14.06	92.4882	24.0582	2.32	1937.7909	200000957	92.5071	24.0545	2
2MASS 06083223+2359391	14.12	92.1341	23.9942	3.93	1940.4535	200000963	92.1533	23.9815	2

^aThese EBs occupy C0 M35 TPFs; the point source 2MASS ID and RA/Dec is supplied followed by the corresponding superstamp TPF and its center pixel coordinates.

Note. — Table flags are as follows: 1) Two primary eclipses observed in C0 (period unconfirmed), 2) Listed in Nardiello et al. 2014,

Table 4. Non-EPIC EBs in Campaign 0

2MASS ID ^a	K_P (mag)	RA (deg)	DEC (deg)	Period (days)	BJD ₀ (BJD-2454833)	Contaminated EPIC	RA (deg)	Dec (deg)	Note Flag
2MASS 06115706+2040109	12.02	92.98780	20.67400	6.81	1942.5413	202060198	92.98965	20.67244	
2MASS 06105541+2037042	9.93	92.72550	20.61270	3.34	1943.4607	202060503	92.73293	20.61952	3
2MASS 07003695+1937177	11.78	105.1540417	19.62186	4.49	1944.2174	202064550	105.15858	19.61459	
2MASS 06181254+2438032	11.33	94.54720	24.63440	7.83	1944.5744	202065879	94.5522	24.63424	
2MASS 06083223+2359391	13.28	97.77700	17.70110	23.79	1945.9438	202071645	97.77472	17.70121	2
2MASS 06404939+2404128	9.65	100.20554	24.07038	7.80	1941.2548	202072624	100.21330	24.07368	
2MASS 06553695+1923084	14.45	103.91137	19.38180	7.60	1944.4453	202072756	103.90250	19.38504	
2MASS 06235708+1820182	12.94	95.98780	18.33850	4.91	1943.226	202083222	95.9835	18.3345	
2MASS 06143505+2343535	14.82	93.646041	23.73158	0.65	1936.3811	202083688	93.646041	23.73158	
2MASS 06262323+1603043	9.36	96.5968	16.0513	0.57	1939.3339	202084063	96.59837	16.06072	
2MASS 06262360+1603385	15.40	97.18890	14.60340	2.03	1943.0423	202084843	97.18514	14.60301	
2MASS 06190294+1828199	14.38	94.76225	18.47227	11.24	1948.14	202085157	94.75625	18.47464	
2MASS 06184418+1821189	13.37	94.68404	18.35525	...	1948.1254	202085278	94.68155	18.35271	1
2MASS 06480648+2323022	16.15	102.02680	23.3839	2.56	1941.4388	202087552	102.02209	23.38287	
2MASS 06230585+2058156	13.55	95.78300	20.97161	0.90	1942.0308	202090938	95.77686	20.97275	2
2MASS 06302365+2622128	13.91	97.5985	26.37016	0.44	1946.7301	202092874	97.60019	26.36851	
2MASS 06290799+2814236	12.89	97.28320	28.23990	5.13	1945.208	202095074	97.28940	28.23426	
2MASS 07021637+1846346	11.50	105.5682083	18.77650	2.41	1942.305	202126863	105.56551	18.77254	
2MASS 06504495+1648335	15.48	102.68690	16.80910	2.92	1942.0928	202127311	102.6836	16.81334	
2MASS 06240232+1613363	11.87	96.00954	16.2267	1.87	1939.2725	202136002	96.0155	16.2275	
2MASS 06235881+1622092	12.73	95.9949	16.3690	2.51	1937.4132	202136015	95.98770	16.36856	
2MASS 06402291+1559465	13.19	97.29830	16.6421	5.20	1943.0525	202136063	97.30045	16.64588	
2MASS 06185304+1840323	13.68	100.09530	15.9961	5.74	1945.3597	202136445	100.09492	15.99292	
2MASS 06185243+1840339	11.35	94.71887	18.67119	3.37	1944.0126	202137030	94.72101	18.67565	
2MASS 06083624+2347222	13.10	92.15095	23.78966	6.14	1944.5813	202137637	92.15124	23.79245	
2MASS 06080534+2352495	15.05	92.0220	23.8805	0.73	1939.5807	202137653	92.02741	23.88216	
2MASS 06245004+1813328	14.33	96.20833	18.22583	1.01	1936.5550	202137708	96.21516	18.23077	
2MASS 06190708+2458234	13.65	94.77945	24.97306	4.45	1942.7764	202138912	94.78377	24.97246	
2MASS 06172371+2539374	13.75	94.34867	25.66047	2.77	1942.0306	202139017	94.34667	25.66506	

^aThese EBs occupy C0 TPF halo pixels; their eclipses contaminate the noted EPIC target

Note. — Table flags are as follows: 1) Single primary eclipse observed in C0, 2) Two primary eclipses observed in C0 (period unconfirmed), 3) Heartbeat binary candidate.

Table 5. Blended EBs in Campaign 0

EPIC ID (EB)	EPIC ID (blend)
202073348	202073377
202062450	202072972
202071279	202073364
202126863	202126867
202060198	202070263
202073489	202073366
202073489	202073362
202065879	202066041
202065879	202065929

Table 6. K2 C0 Eclipsing Binaries Observed by KELT-North

KELT ID	EPIC	K_P (mag)	RA (deg)	Dec (deg)	Period (days)	BJD ₀ (BJD-2454833)
KN 05E09313	202072963	11.40	104.37154	20.18725	4.209922	1941.5103
KN 04E010922	202073097	9.60	91.09233	20.53502	0.972411	1941.9621
KN 04E006640	202060541	10.30	94.08259	20.91274	4.049160	1944.4214
KN 04E102374	202071266	12.50	91.33042	22.54782	2.593621	1944.18
KN 04E005219	202072961	9.30	100.12564	22.91052	4.097024	1945.3702
KN 04E031147	202073238	11.80	90.60747	23.10947	0.791658	1941.5186
KN 04E019375	202060135	9.90	90.36692	23.14098	2.865379	1943.2567
KN 04E046126	202060752	10.80	92.8667	23.2317	0.770391	1941.4077
KN 04E016313	202073186	10.40	94.11483	23.312	1.224829	1941.7959
KN 04E054729	202072978	12.20	100.26213	23.8078	4.885995	1944.6566
KN 04E110687	202073361	11.10	90.25184	23.93759	0.361833	1941.41
KN 04E006288	202072958	10.50	94.19764	24.07841	4.024547	1942.6683
KN 04E069591	202072991	10.20	95.003	26.34982	5.495907	1945.3442
KN 04E039600	202073144	11.10	100.21498	26.74048	1.550610	1941.7757
KN 04E045879	202073307	12.60	92.95463	27.00535	0.505216	1941.7346
KN 04E079988	202073346	12.50	99.31727	27.10678	0.384243	1941.459
KN 04E040654	202073353	12.00	92.6719	27.39488	0.371250	1941.5099
KN 04E065527	202073266	12.10	96.92732	27.4025	0.689607	1941.9902

Note. — Table showing EBs that have light curves from the KELT survey. Ephemeris from Tables 1 and 2. See Section 6 for details.

Table 7. Eccentric EBs in Campaign 0

EPIC ID	e	ω
202072430	0.633	2.890
202091404	0.563	2.726
202062176	0.447	3.464
202071945	0.380	3.733
202071505	0.294	3.245
202071994	0.247	2.884
202068807	0.226	3.3310
202072596	0.150	3.3911

Note. — Table listing the most eccentric EBs in C0. Eccentricities calculated using the methods described in Prša et al. (in prep). See Section 7 for details.

Table 8. Planet Candidates

Parameter	202072704	2MASS 06101557+2436535
2MASS	06455102+1712250	06101557+2436535
K_P (mag)	11.4	13.0
RA (deg)	101.4626	92.5648
Dec (deg)	17.2069	24.6148
P (days)	2.65 ^a	7.5559 ^a
Epoch (MJD)	2456771.13445 \pm 0.00029	2456776.87137 ^{+0.00089} _{-0.00087}
Duration (hrs)	3.202 ^{+0.055} _{-0.038}	3.946 ^{+0.038} _{-0.036}
b	0.676 ^{+0.033} _{-0.055}	0.00 \pm 0.31
i (deg)	81.6 ^{+1.0} _{-0.72}	89.12 ^{+0.62} _{-0.87}
R_p/R_*	0.0814 ^{+0.0016} _{-0.0020}	0.0791 ^{+0.0012} _{-0.00085}
a/R_*	4.66 ^{+0.22} _{-0.16}	14.22 ^{+0.33} _{-0.85}

^aThe period was fixed.

Note. — TAP model fit parameters for the two exoplanet candidates described in Section 8; circular orbits have been assumed.